

Research Article

# Nonlinear Vibration of Single-Walled Carbon Nanotubes on Winkler and Pasternak Foundations in a Magneto-Thermal Environment Under the Influence of Casimir Force

Haruna Egbunu Abubakar<sup>1,\*</sup> , Ahmed Amoo Yinusa<sup>2</sup> ,  
Musbau Gbeminiyi Sobamowo<sup>2</sup> , Obanishola Mufutau Sadiq<sup>1</sup>

<sup>1</sup>Civil and Environmental Engineering Department, University of Lagos, Lagos, Nigeria

<sup>2</sup>Mechanical Engineering Department, University of Lagos, Lagos, Nigeria

## Abstract

Nanotubes are known to have the strongest and stiffest fibers with exceptional tensile strength and higher modulus of elasticity, researchers have been very interested in studying their nonlinear vibrations. Nonetheless, using nanotubes to partially substitute reinforcing material has emerged as a revolutionary approach for applications of the future. This work examines the nonlinear vibration study of single-walled carbon (NTs) with geometric imperfection supported on linear and nonlinear Winkler and Pasternak Foundations in a thermal-magnetic-electrostatic environment under the influence of Casimir Force. The nonlinear mathematical model for this work is formulated using the Hamilton principle, Euler-Bernoulli elasticity theory, and non-local elasticity beam theory. The Galerkin decomposition approach is used directly to break down the nonlinear partial differential equation of motions into two separate components, that is spatial and temporal parts of nonlinear duffing equations of motions. An approximate analytical expression of the fundamental natural frequency is presented by modern asymptotic approach namely Iteration Perturbation Method (IPM). The method is used to solve the resulting nonlinear mathematical model and the following solutions were obtained that is the natural frequency of vibration, nonlinear frequency ratio and dynamic response analysis. Moreso, parametric study was conducted on the obtained semi-analytical solutions and the effects of the following parameters such as magnetic, thermal, electrostatic force, Van der Waals force, Casimir force, linear foundation, nonlinear foundation, Pasternak foundation and mass on stability and dynamic responses on four different boundary conditions considered. Afterwards, the outcomes are then compared with existing literature and found to be completely consistent.

## Keywords

Magnetic, Thermal, Iteration Perturbation, Casimir, Van Der Waal, Elastic Foundation, Electrostatic Force, Single-Walled Carbon Nanotubes

## 1. Introduction

Nonlinear vibration analysis of nanotubes has fascinated strong attention from the researchers due to their stiffest and

strongest known fibers with excellent tensile strength. However, the purpose of using nanotubes as a partial replacement for re-

\*Corresponding author: [egbunu.haruna.abubakar@gmail.com](mailto:egbunu.haruna.abubakar@gmail.com) (Haruna Egbunu Abubakar)

**Received:** 1 February 2025; **Accepted:** 22 March 2025; **Published:** 29 April 2025



Copyright: © The Author(s), 2025. Published by Science Publishing Group. This is an **Open Access** article, distributed under the terms of the Creative Commons Attribution 4.0 License (<http://creativecommons.org/licenses/by/4.0/>), which permits unrestricted use, distribution and reproduction in any medium, provided the original work is properly cited.

inforcement material has become a novelty in tomorrow's applications. Nanotube reinforcement composites (NTRC), which are created by initiating aligned nanotubes to the polymer matrix will likely expand the application of nanotubes. Some researched investigations have been outlined to divulge mechanical behaviors of (NTRC) structures. [1] modeled the nonlinear partial differential equation of motion by presenting a vibration analysis of SWCNTs using the Hamilton principle, Euler-Bernoulli beam theory, and Eringen's non-local elastic theory. The model is then resolved using the cosine after treatment approach and the differential transformation method. [2] studied free vibrational analysis of embedded SWCNTs under longitudinal magnetic field based on non-local strain gradient theory and Euler-Bernoulli beam model. They also used Galerkin and the equivalent linearization methods to obtain stability. Thereafter, simulation was conducted on the parameters in the nonlinear model. [3] investigated the free vibrations of SWCNTs under the theory of non-local elasticity, and the differential quadrature method is used to solve the resultant nonlinear partial differential equation. [4] analyzed the dynamic response of a single-walled carbon nanotube under Euler-Bernoulli beam theory and Eringen's non-local elastic theory with various boundary conditions. After applying dimensionless parameters to the duffing equation of motion, the governing non-linear mathematical model is broken down using the Galerkin decomposition approach. The Homotopy Perturbation Method is then used to solve the resultant nonlinear duffing equation. [5] investigated SWCNTs' nonlinear force vibration under the influence of the Casimir force using Hamiltonian principles and Eringen non-local theory. After applying the Galerkin decomposition approach to the resultant nonlinear duffing equation, a nonlinear mathematical model was created and solved using the Homotopy Perturbation approach. Since they argue for both the concrete's compression and tensile zones, the stability and dynamic response simulation findings turn out to be accurate. [6] examined the stability and flow-induced vibrations of SWCNTs placed in biological soft tissue using the Kelvin-Voigt foundation. The differential transformation technique is used to solve the nonlinear problem that is created using Hamilton's concept. [7] created a non-local strain gradient anisotropic elastic shell nonlinear model to address the vibration of pinned-pinned supports SWCNTs under the Mindlin strain gradient theory, Eringen nonlocal elasticity theory, and Sanders-Koiter shell theory for strain-displacement. Consequently, the parameters are used in the numerical simulations. [8] examined stepped nano-beams immersed in the elastic medium using nonlinear free vibration analysis based on Hamilton's principle and Eringen's nonlocal elasticity theory. Using the perturbation approach once more, the mathematical model was solved. The outcome showed that the elastic medium coefficient decreased vibrational amplitudes, while the nonlocal parameter had a negative influence on frequency. [9] determined how boundary circumstances affected the SWCNT's free vibrations. Following that, the nonlinear governing equation is modeled using Flügge's shell dynamic equations. Additionally, the vibrational frequency equation is determined in typical eigen-

value form using the wave propagation technique. The findings are displayed visually and contrasted with those found in the literature. [10] employed the differential transform method and the cosine after-treatment technique to analyze the nonlinear vibrations of a SWNT with multiple layers on elastic media in a thermal-magnetic environment using the Euler-Bernoulli beam model and nonlocal elasticity theory. This method proved to be very useful for designing CNTs in thermal and magnetic environments. [11] provided a study of laminated composite panels that are flat, concave, and convex and reinforced with carbon nanotubes. Consequently, they analyzed the model using the numerical homogenization of finite element technique, and the outcomes are contrasted with those of traditional composite materials according to various end circumstances. [12] examined the vibrational behavior of fluidic conveying SWCNTs using the differential transform technique and the theories of thermo-elastic mechanics, non-local elasticity, and Euler-Bernoulli beams to describe the system that rested on an elastic medium with clamped-clamped and pinned-pinned supports. [13] discussed using the continuum technique for free vibrational analysis of pinned-pinned supports, including SWCNTs and DWCNTs. Therefore, in the free vibrational analysis of single-walled and double-walled carbon nanotubes, the accuracy of beam models and standard 2D shell models. [14] investigated the nonlinear vibration analysis of a single-walled carbon nanotube with a longitudinal magnetic field utilizing Eringen's Non-local Elasticity theory and Euler-Bernoulli Beam theory to create a nonlinear model, which is then solved using the finite element technique. [15] examined single-wall carbon nanotubes with metallic, semi-conducting, and (6, 5) chirality molar absorbance coefficients. In addition to being independent of the diameter distribution and the electrical kinds of single wall carbon nanotubes, the majority of coefficients have values that fall between 2 and  $5 \times 10^9 \text{ /mL mol}^{-1} \text{ cm}^{-1}$ . Lastly, their coefficient is independent of chirality and electrical kinds and is reliant on the length of single wall carbon nanotubes. [16] examined free vibrational analysis of Single-Walled Carbon Nanotubes with exponentially changing stiffness under nonlocal and Euler-Bernoulli beam theory to model the system, and the differential quadrature method was used to solve the model after converting it to a generalized eigenvalue problem. The results demonstrate that, in contrast to other literature, the solutions obtained using the differential quadrature method converge quickly. [17] examined the various stability of SWCNTs in chiral, armchair, and zigzag configurations lying on elastic media exposed to both high and low temperatures. Once more, surface factors like surface energy and surface residual stresses are taken into account while modeling, and the outcomes are confirmed by another research. [18] examined SWCNT vibrational analysis under a single variable shear deformation beam theory, while also subjected to thermal conditions and an axial or longitudinal magnetic field. The gradient, non-local, and Hamilton's principle are used to build the mathematical model. [19] examined the vibrations of implanted multi-walled branching carbon nanotubes with nanofluid conveyance on Winkler-Pasternak medium

in a thermal-magnetic environment. The nonlinear governing mathematical model is developed using Euler-Bernoulli beam theory, Hamilton's principle, and nonlocal elasticity theory. It is then tied to the energy equations of the vibrational models and Navier-Stoke's equations using multi-dimensional numerical PDE solvers in conjunction with MATLAB PDE tools. The parameters in the solved duffing equation are also subjected to numerical simulations in accordance with this.

## 2. Governing Mathematical Model Equations

Figure 1 illustrates the problem formulation, which is a single-walled carbon nanotube supported by a linear and nonlinear Winklers and Pasternak foundation. The problem is

modeled using Hamilton's principle, Euler-Bernoulli beam theory, and Eringen's nonlocal elasticity beam theory. The following is the longitudinal magnetic field:

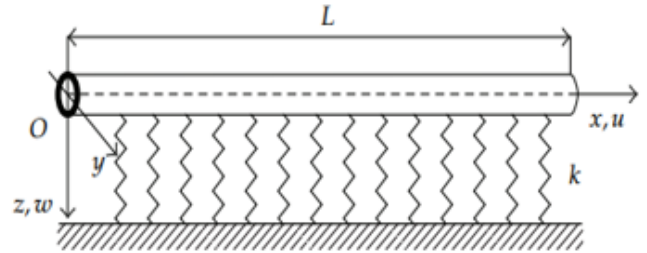


Figure 1. Model of an embedded single-walled carbon nanotube.

$$F_V EI \frac{\partial^4 w}{\partial x^4} + m \frac{\partial^2 w}{\partial t^2} - \eta H_x^2 A \frac{\partial^2 w}{\partial x^2} + K w - (e_0 a)^2 \frac{\partial^2}{\partial x^2} \left( m \frac{\partial^2 w}{\partial t^2} - \eta H_x^2 A \frac{\partial^2 w}{\partial x^2} + K w \right) = 0 \quad (1)$$

The Winklers foundation, both linear and nonlinear, indicates, However,  $K w = k_1 w + k_3 w^3$ , where  $k_1 w$  is linear Winkler-type and  $k_3 w^3$  is non-linear Winkler-type. Substituting back into equation (1) gives:

$$EI \frac{\partial^4 w}{\partial x^4} + m \frac{\partial^2 w}{\partial t^2} - \eta H_x^2 A \frac{\partial^2 w}{\partial x^2} + k_1 w + k_3 w^3 - (e_0 a)^2 \frac{\partial^2}{\partial x^2} \left( m \frac{\partial^2 w}{\partial t^2} - \eta H_x^2 A \frac{\partial^2 w}{\partial x^2} + k_1 w + k_3 w^3 \right) = 0 \quad (2)$$

The concept also incorporates a Pasternak-type foundation that serves as;  $k_p \frac{\partial^2 w}{\partial x^2}$ , initial stresses as  $\sigma_x^0 \frac{\partial^2 w}{\partial x^2}$ , parameter induced by residual surface stress as  $H_s \frac{\partial^2 w}{\partial x^2}$  and change in temperature is  $EA \alpha T \frac{\partial^2 w}{\partial x^2}$  as well as the electrostatic force acting on the system, van der Waal force and Casimir force which are denoted as;  $F_E$  and  $F_C$ . Substituting back into equation (2) yield;

$$EI \frac{\partial^4 w}{\partial x^4} + m \frac{\partial^2 w}{\partial t^2} - \eta H_x^2 A \frac{\partial^2 w}{\partial x^2} + k_1 w + k_3 w^3 - EA \alpha T \frac{\partial^2 w}{\partial x^2} - k_p \frac{\partial^2 w}{\partial x^2} - (e_0 a)^2 \frac{\partial^2}{\partial x^2} \left( m \frac{\partial^2 w}{\partial t^2} - \eta H_x^2 A \frac{\partial^2 w}{\partial x^2} + k_1 w + k_3 w^3 - EA \alpha T \frac{\partial^2 w}{\partial x^2} + \sigma_x^0 \frac{\partial^2 w}{\partial x^2} + H_s \frac{\partial^2 w}{\partial x^2} + k_p \frac{\partial^2 w}{\partial x^2} \right) = F_E + F_V + F_C + (e_0 a)^2 \frac{\partial^2 w}{\partial x^2} (F_E + F_V + F_C) \quad (3)$$

Where, Electrostatic force, van der Waal force and Casimir force are given as:

$$F_E = \frac{1}{2} \frac{b \epsilon V^2}{(d_o - w)^2} \left( 1 + f \left( \frac{d_o - w}{b} \right) \right), \quad F_V = \frac{A b}{6 \pi (d_o - w)^2} \quad \text{and} \quad F_C = \frac{\pi^3 \hbar c b}{240 (d_o - w)^4}$$

Substituting them into equation (3) becomes;

$$\begin{aligned}
& EI \frac{\partial^4 w}{\partial x^4} + m_c \frac{\partial^2 w}{\partial t^2} + k_1 w + k_3 w^3 - \left( \frac{EA}{2L} \int_0^L \left( \frac{\partial Z_o}{\partial x} \frac{\partial w}{\partial x} + \left( \frac{\partial w}{\partial x} \right)^2 \right) dx \right) \left( \frac{\partial^2 Z_o}{\partial x^2} + \frac{\partial^2 w}{\partial x^2} \right) \\
& - \left( EA \alpha_x T + \eta A H_x^2 + k_p \right) \frac{\partial^2 w}{\partial x^2} + (e_o a)^2 \left[ \frac{EA}{2L} \int_0^L \left( \frac{\partial Z_o}{\partial x} \frac{\partial w}{\partial x} + \left( \frac{\partial w}{\partial x} \right)^2 \right) dx \right] \left( \frac{\partial^4 Z_o}{\partial x^4} + \frac{\partial^4 w}{\partial x^4} \right) \\
& - \left( EA \alpha_x T + \eta A H_x^2 + k_p \right) \frac{\partial^4 w}{\partial x^4} \right] \\
& = \frac{1}{2} \frac{b \varepsilon V^2}{(d_o - w)^2} \left( 1 + f \left( \frac{d_0 - w}{b} \right) \right) + \frac{Ab}{6\pi (d_o - w)^2} + \frac{\pi^3 \bar{h} c b}{240 (d_o - w)^4} \\
& + (e_o a)^2 \left[ \frac{b \varepsilon V^2}{(d_o - w)^4} \left( 3 + f \left( \frac{d_0 - w}{b} \right) \right) + \frac{Ab}{\pi (d_o - w)^4} + \frac{\pi^3 \bar{h} c b}{20 (d_o - w)^6} \right]
\end{aligned} \tag{4}$$

When equation (4)'s right-hand side is solved, the result is:

$$\begin{aligned}
& EI \frac{\partial^4 w}{\partial x^4} + m_c \frac{\partial^2 w}{\partial t^2} + k_1 w + k_3 w^3 - \left( \frac{EA}{2L} \int_0^L \left( \frac{\partial Z_o}{\partial x} \frac{\partial w}{\partial x} + \left( \frac{\partial w}{\partial x} \right)^2 \right) dx \right) \left( \frac{\partial^2 Z_o}{\partial x^2} + \frac{\partial^2 w}{\partial x^2} \right) \\
& - \left( EA \alpha_x T + \eta A H_x^2 + k_p \right) \frac{\partial^2 w}{\partial x^2} + (e_o a)^2 \left[ \frac{EA}{2L} \int_0^L \left( \frac{\partial Z_o}{\partial x} \frac{\partial w}{\partial x} + \left( \frac{\partial w}{\partial x} \right)^2 \right) dx \right] \left( \frac{\partial^4 Z_o}{\partial x^4} + \frac{\partial^4 w}{\partial x^4} \right) \\
& - \left( EA \alpha_x T + \eta A H_x^2 + k_p \right) \frac{\partial^4 w}{\partial x^4} \right] = \\
& \frac{\lambda_1}{(1-W)} + \frac{\lambda_2}{(1-W)^2} + \frac{\lambda_3}{(1-W)^3} + \frac{\lambda_4}{(1-W)^4} + \frac{\lambda_6}{(1-W)^6}
\end{aligned} \tag{5}$$

Through expanding series solution, equation (5)'s right hand side (RHS) becomes:

$$\frac{\lambda_1}{(1-W)} = \lambda_1 \left( 1 + W + W^2 + W^3 + W^4 + W^5 + W^6 + O(W^7) \right) \tag{6}$$

$$\frac{\lambda_2}{(1-W)^2} = \lambda_2 \left( 1 + 2W + 3W^2 + 4W^3 + 5W^4 + 6W^5 + 7W^6 + O(W^7) \right) \tag{7}$$

$$\frac{\lambda_3}{(1-W)^3} = \lambda_3 \left( 1 + 3W + 6W^2 + 10W^3 + 15W^4 + 21W^5 + 28W^6 + O(W^7) \right) \tag{8}$$

$$\frac{\lambda_4}{(1-W)^4} = \lambda_4 \left( 1 + 4W + 10W^2 + 20W^3 + 35W^4 + 56W^5 + 84W^6 + O(W^7) \right) \tag{9}$$

$$\frac{\lambda_6}{(1-W)^6} = \lambda_6 \left( 1 + 6W + 21W^2 + 56W^3 + 126W^4 + 252W^5 + 462W^6 + O(W^7) \right) \tag{10}$$

Substituting equation (6), (7), (8), (9) and (10) into equation (5) produce;

$$\begin{aligned}
 EI \frac{\partial^4 w}{\partial x^4} + m_c \frac{\partial^2 w}{\partial t^2} + k_1 w + k_3 w^3 - \left( \frac{EA}{2L} \int_0^L \left( \frac{\partial Z_o}{\partial x} \frac{\partial w}{\partial x} + \left( \frac{\partial w}{\partial x} \right)^2 \right) dx \right) \left( \frac{\partial^2 Z_o}{\partial x^2} + \frac{\partial^2 w}{\partial x^2} \right) \\
 - \left( EA \alpha_x T + \eta A H_x^2 + k_p \right) \frac{\partial^2 w}{\partial x^2} + (e_o a)^2 \left[ - \left( \frac{EA}{2L} \int_0^L \left( \frac{\partial Z_o}{\partial x} \frac{\partial w}{\partial x} + \left( \frac{\partial w}{\partial x} \right)^2 \right) dx \right) \left( \frac{\partial^4 Z_o}{\partial x^4} + \frac{\partial^4 w}{\partial x^4} \right) \right. \\
 \left. - \left( EA \alpha_x T + \eta A H_x^2 + k_p \right) \frac{\partial^4 w}{\partial x^4} \right] = \\
 \left[ \lambda_1 \left( 1 + W + W^2 + W^3 + W^4 + W^5 + W^6 + O(W^7) \right) + \lambda_2 \left( 1 + 2W + 3W^2 + 4W^3 + \right. \right. \\
 \left. \left. 5W^4 + 6W^5 + 7W^6 + O(W^7) \right) \right. \\
 \left. + \lambda_3 \left( 1 + 3W + 6W^2 + 10W^3 + 15W^4 + 21W^5 + 28W^6 + O(W^7) \right) + \lambda_4 \left( 1 + 4W + 10W^2 + \right. \right. \\
 \left. \left. 20W^3 + 35W^4 + \right. \right. \\
 \left. \left. 56W^5 + 84W^6 + O(W^7) \right) \right. \\
 \left. + \lambda_6 \left( 1 + 6W + 21W^2 + 56W^3 + 126W^4 + 252W^5 + 462W^6 + O(W^7) \right) \right]
 \end{aligned} \quad (11)$$

The parameters in the model are defined as:

$I$ : Second moment of inertia

$E$ : Young modulus of elasticity

$m$ : Tube mass per unit length

$\eta$ : Magnetic field permeability

$H_x$ : Magnetic field strength

$A$ : Cross sectional area

$k$ : Foundation stiffness

$e_0$ : Nonlocal material constant

$a$ : Internal characteristic length of the nanotube

$w$ : Displacement

$L$ : Length of the tube

$t$ : Time

$x$ : Cartesian axis

$\bar{h}$ : Plank constant

$c$ : Speed of sound

$b$ : Width of the tube

$d$ : Diameter of the tube

Nevertheless, the following displacement boundary conditions are applied to this investigation of the dynamic response of single-walled carbon nanotubes:

Pinned-Pinned supported (P-P) nanotube,

$$w(0, t) = 0, \quad \frac{\partial^2 w(0, t)}{\partial x^2} = 0, \quad w(L, t) = 0, \quad \frac{\partial^2 w(L, t)}{\partial x^2} = 0. \quad (12)$$

Clamped-Clamped supported (C-C) nanotube,

$$w(0, t) = 0, \quad \frac{\partial w(0, t)}{\partial x} = 0, \quad w(L, t) = 0, \quad \frac{\partial w(L, t)}{\partial x} = 0. \quad (13)$$





Clamped-Pinned supported (C-P) nanotube,

$$w(0, t) = 0, \quad \frac{\partial w(0, t)}{\partial x} = 0, \quad w(L, t) = 0, \quad \frac{\partial^2 w(L, t)}{\partial x^2} = 0. \quad (14)$$

Clamped-Free supported (C-F) nanotube,

$$w(0,t) = 0, \quad \frac{\partial^2 w(0,t)}{\partial x^2} = 0, \quad w(L,t) = 0, \quad \frac{\partial^3 w(L,t)}{\partial x^3} = 0. \quad (15)$$

**Table 1.** Shown the fundamental functions that match the aforementioned boundary constraints.

Cases	Mode shape,	$\phi(x)$	Value of $\beta$
Pinned-Pinned supports	 showing pinned-pinned supports.	$\sin\left(\frac{\beta x}{L}\right)$	$\pi$
Clamped-Clamped supports	 showing clamped-clamped supports.	$\left(\cosh\left(\frac{\beta x}{L}\right) - \cos\left(\frac{\beta x}{L}\right)\right) - \left(\frac{\sinh \beta + \sin \beta}{\cosh \beta - \cos \beta}\right) \left(\sinh\left(\frac{\beta x}{L}\right) - \sin\left(\frac{\beta x}{L}\right)\right)$	4.730041
Clamped-Pinned supports	 showing clamped-pinned supports.	$\left(\cosh\left(\frac{\beta x}{L}\right) - \cos\left(\frac{\beta x}{L}\right)\right) - \left(\frac{\cosh \beta - \cos \beta}{\sinh \beta - \sin \beta}\right) \left(\sinh\left(\frac{\beta x}{L}\right) - \sin\left(\frac{\beta x}{L}\right)\right)$	3.926602
Clamped-Free supports	 showing clamped-free supports.	$\left(\cosh\left(\frac{\beta x}{L}\right) - \cos\left(\frac{\beta x}{L}\right)\right) - \left(\frac{\cosh \beta + \cos \beta}{\sinh \beta + \sin \beta}\right) \left(\sinh\left(\frac{\beta x}{L}\right) - \sin\left(\frac{\beta x}{L}\right)\right)$	1.87510

Using a few dimensionless parameters, equation (11) is conveniently rearranged into dimensionless form. Included in these dimensionless variables are:

$$\begin{aligned}
 X &= \frac{x}{L}, & W &= \frac{w}{d_0}, K_1 = \frac{k_1 L^4}{EI}, & \tau &= t \frac{h}{L^2} \sqrt{\frac{E}{12\rho}}, & H_a &= \frac{\eta A H_x^2 L^2}{EI}, \\
 \lambda_3 &= \frac{L^4}{EI d_0} \left( \frac{AbL^4}{6EI\pi d_0^4} + \frac{bf\varepsilon V^2 (e_0 a)^2}{d_0^3} \right), & \lambda_4 &= \frac{L^4}{EI d_0} \left( \frac{\pi^2 hcbL^4}{240EI d_0^5} + \frac{(e_0 a)^2 \left( \frac{3b\varepsilon V^2 + Ab}{\pi} \right)}{d_0^4} \right), \\
 \lambda_6 &= \frac{\pi^2 hcbL^4}{20EI d_0^7}, & K_3 &= \frac{k_3 L^4 d_0^2}{EI}, & \alpha_1 &= \frac{16d_0^2}{h_2}, & K_p &= \frac{k_p L^2}{EI}, & \theta &= \frac{EA\alpha_x TL^2}{EI}
 \end{aligned} \quad (16)$$

Equation (17) below is the dimensionless equation of motion when Eq. (16) is substituted into equation (11), yield:

$$\begin{aligned}
 & \frac{\partial^4 W}{\partial X^4} + \frac{\partial^2 W}{\partial \tau^2} + K_1 W + K_3 W^3 - \left( \alpha_1 \int_0^1 \left( \frac{\partial Z_o}{\partial X} \frac{\partial W}{\partial X} + \left( \frac{\partial W}{\partial X} \right)^2 \right) dX \right) \left( \frac{\partial^2 Z_o}{\partial X^2} + \frac{\partial^2 W}{\partial X^2} \right) - (\Delta T + H_a + K_p) \frac{\partial^2 W}{\partial X^2} \\
 & + (e_0 a)^2 \left[ \alpha_2 \frac{\partial^4 W}{\partial X^2 \partial \tau^2} + K_1 \frac{\partial^2 W}{\partial X^2} + 6K_3 W \left( \frac{\partial W}{\partial X} \right)^2 + 3K_3 W^2 \left( \frac{\partial^2 W}{\partial X^2} \right) \right. \\
 & \left. - \left( \alpha_1 \int_0^1 \left( \frac{\partial Z_o}{\partial X} \frac{\partial W}{\partial X} + \left( \frac{\partial W}{\partial X} \right)^2 \right) dX \right) \left( \frac{\partial^4 Z_o}{\partial X^4} + \frac{\partial^4 W}{\partial X^4} \right) \right. \\
 & \left. - (\Delta T + H_a + K_p) \frac{\partial^4 W}{\partial W^4} \right] \\
 & = \left( (\lambda_1 + \lambda_2 + \lambda_3 + \lambda_4 + \lambda_6) + (\lambda_1 + 2\lambda_2 + 3\lambda_3 + 4\lambda_4 + 6\lambda_6)W + \left( \frac{\lambda_1 + 3\lambda_2 + 6\lambda_3}{+10\lambda_4 + 21\lambda_6} \right)W^2 \right) \\
 & + (\lambda_1 + 4\lambda_2 + 10\lambda_3 + 20\lambda_4 + 56\lambda_6)W^3 + (\lambda_1 + 5\lambda_2 + 15\lambda_3 + 35\lambda_4 + 126\lambda_6)W^4 \\
 & + (\lambda_1 + 6\lambda_2 + 21\lambda_3 + 56\lambda_4 + 252\lambda_6)W^5 + (\lambda_1 + 7\lambda_2 + 28\lambda_3 + 84\lambda_4 + 462\lambda_6)W^6
 \end{aligned} \quad (17)$$

## 2.1. Transforming the Governing Equation Using Galerkin Composition Method from PDE to ODE

The Galerkin decomposition approach is used to transform Eq. (17) into a nonlinear duffing equation. As demonstrated, this process enables the deflection of the SWCNT's to be expressed as a product of two independent functions.

$$w(X, \tau) = u(\tau) \phi(X) \quad (18)$$

Where a function  $\phi(X)$ , chosen to meet the end supports

conditions requirements is shown in Table 1. Remember that the Galerkin transform, one parameter at a time, is defined as follows:

$$\int_0^1 R(X, \tau) \phi(X) dX \quad (19)$$

The nonlinear equation is  $R(X, \tau)$ . The decomposition equation is as follows when Eq. (19) is applied to the governing equations:

$$\int_0^1 \left[ \begin{aligned} & \left( \frac{\partial^4 W}{\partial X^4} + \frac{\partial^2 W}{\partial \tau^2} + K_1 W + K_3 W^3 - \left( \alpha_1 \int_0^1 \left( \frac{\partial Z_o}{\partial X} \frac{\partial W}{\partial X} + \left( \frac{\partial W}{\partial X} \right)^2 \right) dX \right) \left( \frac{\partial^2 Z_o}{\partial X^2} + \frac{\partial^2 W}{\partial X^2} \right) \right. \\ & \left. - (\Delta T + H_a + K_p) \frac{\partial^2 W}{\partial X^2} \right. \\ & \left. \left( \alpha_2 \frac{\partial^4 W}{\partial X^2 \partial \tau^2} + K_1 \frac{\partial^2 W}{\partial X^2} + 6K_3 W \left( \frac{\partial W}{\partial X} \right)^2 + 3K_3 W^2 \left( \frac{\partial^2 W}{\partial X^2} \right) \right) \right. \\ & \left. - \left( \alpha_1 \int_0^1 \left( \frac{\partial Z_o}{\partial X} \frac{\partial W}{\partial X} + \left( \frac{\partial W}{\partial X} \right)^2 \right) dX \right) \left( \frac{\partial^4 Z_o}{\partial X^4} + \frac{\partial^4 W}{\partial X^4} \right) \right. \\ & \left. - (\Delta T + H_a + K_p) \frac{\partial^4 W}{\partial W^4} \right) \phi(X) dX \\ & = \left( (\lambda_1 + \lambda_2 + \lambda_3 + \lambda_4 + \lambda_6) + (\lambda_1 + 2\lambda_2 + 3\lambda_3 + 4\lambda_4 + 6\lambda_6)W + \left( \frac{\lambda_1 + 3\lambda_2 + 6\lambda_3}{+10\lambda_4 + 21\lambda_6} \right) W^2 \right. \\ & \left. + (\lambda_1 + 4\lambda_2 + 10\lambda_3 + 20\lambda_4 + 56\lambda_6)W^3 + (\lambda_1 + 5\lambda_2 + 15\lambda_3 + 35\lambda_4 + 126\lambda_6)W^4 \right. \\ & \left. + (\lambda_1 + 6\lambda_2 + 21\lambda_3 + 56\lambda_4 + 252\lambda_6)W^5 + (\lambda_1 + 7\lambda_2 + 28\lambda_3 + 84\lambda_4 + 462\lambda_6)W^6 \right) \end{aligned} \right] \phi(X) dX \quad (20)$$

After integrating and combining the temporal component as a coefficient, the SWCNT's Duffing equation is as follows:

$$m\ddot{u} + \sum_{i=0}^6 \Gamma_i u^i = 0 \quad (21)$$

Expanding equation (21), gives;

$$m\ddot{u} + \Gamma_0 + \Gamma_1 u + \Gamma_2 u^2 + \Gamma_3 u^3 + \Gamma_4 u^4 + \Gamma_5 u^5 + \Gamma_6 u^6 = 0 \quad (22)$$

Subject to  $a = a$ ,  $\dot{u} = 0$ ,

## 2.2. Coefficient of Duffing Equation

Equation (22) coefficients are:

$$m = \int_0^1 \left[ \phi(X) + \alpha_2 \frac{d^2 \phi(X)}{dX^2} \right] \phi(X) dX \quad (23)$$

$$\Gamma_0 = - \int_0^1 [\lambda_1 + \lambda_2 + \lambda_3 + \lambda_4 + \lambda_6] \phi(X) dX \quad (24)$$

$$\Gamma_1 = \int_0^1 \left[ \frac{d^4 \phi(X)}{dX^4} + K_1 \phi(X) - (\alpha_1 N) \left( \frac{d^2 \phi(X)}{dX^2} \right) - (\theta + H_a + K_p) \frac{d^2 \phi(X)}{dX^2} + (e_o a)^2 \left( K_1 \frac{d^2 \phi(X)}{dX^2} - (\alpha_1 N) \left( \frac{d^4 \phi(X)}{dX^4} \right) - (\theta + H_a + K_p) \frac{d^4 \phi(X)}{dX^4} \right) - (\lambda_1 + 2\lambda_2 + 3\lambda_3 + 4\lambda_4 + 6\lambda_6) \right] \phi(X) dX \quad (25)$$

$$\Gamma_2 = - \int_0^1 [\lambda_1 + 3\lambda_2 + 6\lambda_3 + 10\lambda_4 + 21\lambda_6] \phi(X) dX \quad (26)$$

$$\Gamma_3 = \int_0^1 \left[ K_3 \phi^3(X) + (e_o a)^2 \left( 6K_3 \phi(X) \left( \frac{d\phi(X)}{dX} \right)^2 + 3K_3 \phi(X)^2 \left( \frac{d^2 \phi(X)}{dX^2} \right) \right) - (\lambda_1 + 4\lambda_2 + 10\lambda_3 + 20\lambda_4 + 56\lambda_6) \right] \phi(X) dX \quad (27)$$

$$\Gamma_4 = - \int_0^1 [\lambda_1 + 5\lambda_2 + 15\lambda_3 + 35\lambda_4 + 126\lambda_6] \phi^5(X) dX \quad (28)$$

$$\Gamma_5 = - \int_0^1 [\lambda_1 + 6\lambda_2 + 21\lambda_3 + 56\lambda_4 + 252\lambda_6] \phi^6(X) dX \quad (29)$$

$$\Gamma_6 = - \int_0^1 [\lambda_1 + 7\lambda_2 + 28\lambda_3 + 84\lambda_4 + 462\lambda_6] \phi^7(X) dX \quad (30)$$

### 3. Method of Iteration Perturbation for Approximation

Iteration and perturbation techniques are coupled to create the Iteration Perturbation Method. This approach works for differential equations that are substantially nonlinear as well as mildly nonlinear issues. The nonlinear equation (22), for example, requires the introduction of a fake parameter  $\varepsilon$  in order to provide an iteration perturbation solution of the governing equation.

Using the iterative perturbation method on equation (22)'s a duffing equation and dividing the result by  $m$  yields:

$$\ddot{u}(t) + \frac{\Gamma_0}{m} + \frac{\Gamma_1}{m} u(t) + \frac{\Gamma_2}{m} u^2(t) + \frac{\Gamma_3}{m} u^3(t) + \frac{\Gamma_4}{m} u^4(t) + \frac{\Gamma_5}{m} u^5(t) + \frac{\Gamma_6}{m} u^6(t) = 0 \quad (31)$$

However, let replace some parameters in equation (31) as:

$$\beta_0 = \frac{\Gamma_0}{m}, \beta_1 = \frac{\Gamma_1}{m}, \beta_2 = \frac{\Gamma_2}{m}, \beta_3 = \frac{\Gamma_3}{m}, \beta_4 = \frac{\Gamma_4}{m}, \beta_5 = \frac{\Gamma_5}{m}, \beta_6 = \frac{\Gamma_6}{m} \quad (32)$$

Substituting equation (32) into equation (31) gives;

$$\ddot{u}(t) + \beta_0 + \beta_1 u(t) + \beta_2 u^2(t) + \beta_3 u^3(t) + \beta_4 u^4(t) + \beta_5 u^5(t) + \beta_6 u^6(t) = 0 \quad (33)$$

The governing equation's iteration perturbation solution can be obtained by introducing an artificial parameter  $\varepsilon$  in the following manner:

$$\frac{d^2 u}{dt^2} + \varepsilon u (\beta_1 + \beta_2 u + \beta_3 u^2 + \beta_4 u^3 + \beta_5 u^4 + \beta_6 u^5) + \varepsilon \beta_0 = 0 \quad (34)$$



Equation (34) can be approximated by:

$$\frac{d^2u}{dt^2} + \varepsilon u \left( \beta_1 + \beta_2 u_0 + \beta_3 u_0^2 + \beta_4 u_0^3 + \beta_5 u_0^4 + \beta_6 u_0^5 \right) + \varepsilon \beta_0 = 0 \quad (35)$$

$$\frac{d^2u}{dt^2} + \varepsilon \beta_1 u + \varepsilon u \left( \beta_2 u_0 + \beta_3 u_0^2 + \beta_4 u_0^3 + \beta_5 u_0^4 + \beta_6 u_0^5 \right) + \varepsilon \beta_0 = 0 \quad (36)$$

Where  $u_0$ , is the first approximation answer. With  $\omega$  representing the unknown angular frequency, the first solution can be considered to be as follows:  $u_0(t) = a \cos(\omega t)$ . Substituting  $u_0$  into equation (36) yields:

$$\frac{d^2u}{dt^2} + \varepsilon \beta_1 u + \varepsilon u \left( \beta_2 (a \cos(\omega t)) + \beta_3 (a \cos(\omega t))^2 + \beta_4 (a \cos(\omega t))^3 + \beta_5 (a \cos(\omega t))^4 + \beta_6 (a \cos(\omega t))^5 \right) + \varepsilon \beta_0 = 0 \quad (37)$$

It can be further simplified as:

$$\frac{d^2u}{dt^2} + \varepsilon \beta_1 u + \varepsilon u \left( \beta_2 a (\cos(\omega t)) + \beta_3 a^2 (\cos(\omega t))^2 + \beta_4 a^3 (\cos(\omega t))^3 + \beta_5 a^4 (\cos(\omega t))^4 + \beta_6 a^5 (\cos(\omega t))^5 \right) + \varepsilon \beta_0 = 0 \quad (38)$$

The equation (38) can be written in the following form after application of combine trigonometry:

$$\frac{d^2u_1}{dt^2} + \varepsilon \beta_1 u + \varepsilon u \left( \left( \frac{5a^5\beta_5}{8} + \frac{3a^3\beta_3}{4} + c_1 a \right) \cos(\omega t) + \left( \frac{a^3\beta_4}{8} + \frac{a^2\beta_2}{2} + \frac{3a^4\beta_4}{8} + \frac{15a^6\beta_6}{32} \right) \cos(2\omega t) + \left( \frac{a^3\beta_3}{4} + \frac{5a^5\beta_5}{16} \right) \cos(3\omega t) + \left( \frac{a^3\beta_4}{8} + \frac{3a^6\beta_6}{16} \right) \cos(4\omega t) + \frac{a^5\beta_5}{16} \cos(5\omega t) + \frac{a^6\beta_6}{32} \cos(6\omega t) + \frac{a^2\beta_2}{2} + \frac{3a^4\beta_4}{8} + \frac{5a^6\beta_6}{16} \right) + \varepsilon \beta_0 = 0 \quad (39)$$

assuming that,

$$u = u_0 + \varepsilon u_1 + \varepsilon^2 u_2 + \dots \quad (40)$$

$$\varepsilon \beta_1 = \omega^2 + \varepsilon c_1 + \varepsilon^2 c_2 + \dots \quad (41)$$

Substituting equation (40) and (41) into equation (39) after picking  $\varepsilon$  in power of one yield:

$$\frac{d^2u_1}{dt^2} + \omega^2 u_1 + \left( \left( \frac{5a^5\beta_5}{8} + \frac{3a^3\beta_3}{4} + c_1 a \right) \cos(\omega t) + \left( \frac{a^3\beta_4}{8} + \frac{a^2\beta_2}{2} + \frac{3a^4\beta_4}{8} + \frac{15a^6\beta_6}{32} \right) \cos(2\omega t) + \left( \frac{a^3\beta_3}{4} + \frac{5a^5\beta_5}{16} \right) \cos(3\omega t) + \left( \frac{a^3\beta_4}{8} + \frac{3a^6\beta_6}{16} \right) \cos(4\omega t) + \frac{a^5\beta_5}{16} \cos(5\omega t) + \frac{a^6\beta_6}{32} \cos(6\omega t) + \frac{a^2\beta_2}{2} + \frac{3a^4\beta_4}{8} + \frac{5a^6\beta_6}{16} \right) + \beta_0 = 0 \quad (42)$$

If the term  $\cos(\omega t)$  exists in equation (42), the final solution will contain the secular term,  $t \cos(\omega t)$ . As a result, this term's coefficient in (42) ought to be zero, giving us:

$$\frac{5a^5\beta_5}{8} + \frac{3a^3\beta_3}{4} + c_1 a = 0 \quad (43)$$

Solving the above equation (43), yields:

$$c_1 = -\left(\frac{5a^4\beta_5}{8} + \frac{3a^2\beta_3}{4}\right) \quad (44)$$

Nonetheless the fundamental frequency of vibration is obtained as:

$$\omega_n = \sqrt{\frac{\eta_1}{m}} = \sqrt{\beta_1} \quad (48)$$

### 3.1. For Stability Analysis of the Model Solution

From equation (41), setting

$$\varepsilon = 1, \quad \beta_1 = \omega^2 + c_1 + \dots = 0 \quad (45)$$

Substituting  $c_1$  into equation (45), gives:

Consequently, the frequency-ratio is obtained as;

$$\frac{\omega_o}{\omega_n} = \sqrt{1 + \frac{1}{\beta_1} \left( \frac{3\beta_3 a^2}{4} + \frac{5\beta_5 a^4}{8} \right)} \quad (49)$$

Substituting value of  $\beta_3, \beta_5$  gives;

$$\frac{\omega_o}{\omega_n} = 1 + \left[ \frac{3a^2 \int_0^1 \left[ K_3 \phi^3(X) + (e_o a)^2 \left( 6K_3 \phi(X) \left( \frac{d\phi(X)}{dX} \right)^2 + 3K_3 \phi(X)^2 \left( \frac{d^2\phi(X)}{dX^2} \right) \right) \right] \phi(X) dX}{-(\lambda_1 + 4\lambda_2 + 10\lambda_3 + 20\lambda_4 + 56\lambda_6)} + \frac{\left( \frac{5a^4 - \int_0^1 [\lambda_1 + 6\lambda_2 + 21\lambda_3 + 56\lambda_4 + 252\lambda_6] \phi^6(X) dX}{8} \right) \phi(X) dX}{4} \right] \quad (50)$$

### 3.2. For Dynamic Response Analysis

Solving equation (42) with secular terms and boundary conditions,  $u_1(t)$  is obtained as:

$$u_1(t) = \frac{1}{1680\omega^2} \left( \begin{aligned} &48a^6\beta_6 \left( \frac{\cos(6\omega t)}{32} + \frac{3\cos(4\omega t)}{16} + \frac{15\cos(2\omega t)}{32} + \frac{5}{16} \right) + \\ &70a^5\beta_5 \left( \frac{\cos(5\omega t)}{16} + \frac{5\cos(3\omega t)}{16} \right) + \left( 96a^6\beta_6 + \frac{112a^3\beta_4}{8} \right) \left( \frac{\cos(4\omega t)}{8} + \frac{\cos(2\omega t)}{2} + \frac{3}{8} \right) + \\ &\left( 175a^5\beta_5 + 210a^3\beta_3 \right) \left( \frac{\cos(3\omega t)}{4} + \frac{3\cos(\omega t)}{4} \right) + \\ &\left( 384a^6\beta_6 + 420a^4\beta_4 + 28a^3\beta_4 + 560a^2\beta_2 \right) \left( \frac{\cos(2\omega t)}{2} + \frac{1}{2} \right) + \\ &\left( 240a^6\beta_6 - 245a^5\beta_5 + 420a^4\beta_4 + (-210\beta_3 - 84\beta_4)a^3 + \frac{560a^2\beta_2 + 1680\beta_0}{768a^6\beta_6 - 840a^4\beta_4 - 56a^3\beta_4 - 1120a^2\beta_2 - 1680\beta_0} \right) \cos(\omega t) - \end{aligned} \right) \quad (51)$$

Adding the obtained series solutions together equation (51) yield;

$$u(t) = u_0(t) + u_1(t) + \dots \quad (52)$$

And also substituting  $u_0(t), u_1(t)$  gives:

$$u(t) = \left[ a \cos(\omega t) + \frac{1}{1680\omega^2} \left( \begin{aligned} &48a^6\beta_6 \left( \frac{\cos(6\omega t)}{32} + \frac{3\cos(4\omega t)}{16} + \frac{15\cos(2\omega t)}{32} + \frac{5}{16} \right) + \\ &70a^5\beta_5 \left( \frac{\cos(5\omega t)}{16} + \frac{5\cos(3\omega t)}{16} \right) + \left( 96a^6\beta_6 + \frac{5\cos(\omega t)}{8} \right) \left( \frac{\cos(4\omega t)}{8} + \frac{\cos(2\omega t)}{2} + \frac{3}{8} \right) + \\ &(175a^5\beta_5 + 210a^3\beta_3) \left( \frac{\cos(3\omega t)}{4} + \frac{3\cos(\omega t)}{4} \right) + \\ &(384a^6\beta_6 + 420a^4\beta_4 + 28a^3\beta_4 + 560a^2\beta_2) \left( \frac{\cos(2\omega t)}{2} + \frac{1}{2} \right) + \\ &\left( 240a^6\beta_6 - 245a^5\beta_5 + 420a^4\beta_4 + (-210\beta_3 - 84\beta_4)a^3 + \right. \\ &\left. 560a^2\beta_2 + 1680\beta_0 \right) \cos(\omega t) - \\ &768a^6\beta_6 - 840a^4\beta_4 - 56a^3\beta_4 - 1120a^2\beta_2 - 1680\beta_0 \end{aligned} \right) \right] \quad (53)$$

Therefore, deflection of four boundary conditions considered are obtained as stated below:

When simple-simple supports, (C-C) are used, deflection turns into;

$$w(x,t) = \left[ a \cos(\omega t) + \frac{1}{1680\omega^2} \left( \begin{aligned} &48a^6\beta_6 \left( \frac{\cos(6\omega t)}{32} + \frac{3\cos(4\omega t)}{16} + \frac{15\cos(2\omega t)}{32} + \frac{5}{16} \right) + \\ &70a^5\beta_5 \left( \frac{\cos(5\omega t)}{16} + \frac{5\cos(3\omega t)}{16} \right) + \left( 96a^6\beta_6 + \frac{5\cos(\omega t)}{8} \right) \left( \frac{\cos(4\omega t)}{8} + \frac{\cos(2\omega t)}{2} + \frac{3}{8} \right) + \\ &(175a^5\beta_5 + 210a^3\beta_3) \left( \frac{\cos(3\omega t)}{4} + \frac{3\cos(\omega t)}{4} \right) + \\ &(384a^6\beta_6 + 420a^4\beta_4 + 28a^3\beta_4 + 560a^2\beta_2) \left( \frac{\cos(2\omega t)}{2} + \frac{1}{2} \right) + \\ &\left( 240a^6\beta_6 - 245a^5\beta_5 + 420a^4\beta_4 + (-210\beta_3 - 84\beta_4)a^3 + \right. \\ &\left. 560a^2\beta_2 + 1680\beta_0 \right) \cos(\omega t) - \\ &768a^6\beta_6 - 840a^4\beta_4 - 56a^3\beta_4 - 1120a^2\beta_2 - 1680\beta_0 \end{aligned} \right) \right] * \sin\left(\frac{\beta x}{l}\right) \quad (54)$$

When clamped-clamped supports, (C-C) are used, deflection turns into;

$$\begin{aligned}
 w(x,t) = & \left( a \cos(\omega t) + \right. \\
 & \left. \frac{1}{1680\omega^2} \left( 48a^6\beta_6 \left( \frac{\cos(6\omega t)}{32} + \frac{3\cos(4\omega t)}{16} + \frac{15\cos(2\omega t)}{32} + \frac{5}{16} \right) + \right. \right. \\
 & \left. 70a^5\beta_5 \left( \frac{\cos(5\omega t)}{16} + \frac{5\cos(3\omega t)}{16} + \frac{5\cos(\omega t)}{8} \right) + \left( 96a^6\beta_6 + 112a^3\beta_4 \right) \left( \frac{\cos(4\omega t)}{8} + \frac{\cos(2\omega t)}{2} + \frac{3}{8} \right) + \right. \\
 & \left. \left( 175a^5\beta_5 + 210a^3\beta_3 \right) \left( \frac{\cos(3\omega t)}{4} + \frac{3\cos(\omega t)}{4} \right) + \right. \\
 & \left. \left( 384a^6\beta_6 + 420a^4\beta_4 + 28a^3\beta_4 + 560a^2\beta_2 \right) \left( \frac{\cos(2\omega t)}{2} + \frac{1}{2} \right) + \right. \\
 & \left. \left( 240a^6\beta_6 - 245a^5\beta_5 + 420a^4\beta_4 + (-210\beta_3 - 84\beta_4)a^3 + 560a^2\beta_2 + 1680\beta_0 \right) \cos(\omega t) - \right. \\
 & \left. \left. \left( 768a^6\beta_6 - 840a^4\beta_4 - 56a^3\beta_4 - 1120a^2\beta_2 - 1680\beta_0 \right) \right) \right) \\
 & * \left( \cosh\left(\frac{\beta x}{l}\right) - \cos\left(\frac{\beta x}{l}\right) - \right. \\
 & \left. \frac{\sinh(\beta) + \sin(\beta)}{\cosh(\beta) - \cos(\beta)} \left( \sinh\left(\frac{\beta x}{l}\right) - \sin\left(\frac{\beta x}{l}\right) \right) \right)
 \end{aligned} \tag{55}$$

When clamped-simple supports, (C-C) are used, deflection turns into;

$$\begin{aligned}
 w(x,t) = & \left( a \cos(\omega t) + \right. \\
 & \left. \frac{1}{1680\omega^2} \left( 48a^6\beta_6 \left( \frac{\cos(6\omega t)}{32} + \frac{3\cos(4\omega t)}{16} + \frac{15\cos(2\omega t)}{32} + \frac{5}{16} \right) + \right. \right. \\
 & \left. 70a^5\beta_5 \left( \frac{\cos(5\omega t)}{16} + \frac{5\cos(3\omega t)}{16} + \frac{5\cos(\omega t)}{8} \right) + \left( 96a^6\beta_6 + 112a^3\beta_4 \right) \left( \frac{\cos(4\omega t)}{8} + \frac{\cos(2\omega t)}{2} + \frac{3}{8} \right) + \right. \\
 & \left. \left( 175a^5\beta_5 + 210a^3\beta_3 \right) \left( \frac{\cos(3\omega t)}{4} + \frac{3\cos(\omega t)}{4} \right) + \right. \\
 & \left. \left( 384a^6\beta_6 + 420a^4\beta_4 + 28a^3\beta_4 + 560a^2\beta_2 \right) \left( \frac{\cos(2\omega t)}{2} + \frac{1}{2} \right) + \right. \\
 & \left. \left( 240a^6\beta_6 - 245a^5\beta_5 + 420a^4\beta_4 + (-210\beta_3 - 84\beta_4)a^3 + 560a^2\beta_2 + 1680\beta_0 \right) \cos(\omega t) - \right. \\
 & \left. \left. \left( 768a^6\beta_6 - 840a^4\beta_4 - 56a^3\beta_4 - 1120a^2\beta_2 - 1680\beta_0 \right) \right) \right) \\
 & * \left( \cosh\left(\frac{\beta x}{l}\right) - \cos\left(\frac{\beta x}{l}\right) - \right. \\
 & \left. \frac{\sinh(\beta) - \sin(\beta)}{\cosh(\beta) - \cos(\beta)} \left( \sinh\left(\frac{\beta x}{l}\right) - \sin\left(\frac{\beta x}{l}\right) \right) \right)
 \end{aligned} \tag{56}$$

When clamped-free supports, (C-F) are used, deflection turns into;

$$w(x,t) = \frac{1}{1680\omega^2} \left( \begin{aligned} & a \cos(\omega t) + \\ & \left( 48a^6\beta_6 \left( \frac{\cos(6\omega t)}{32} + \frac{3\cos(4\omega t)}{16} + \frac{15\cos(2\omega t)}{32} + \frac{5}{16} \right) + \right. \\ & \left. 70a^5\beta_5 \left( \frac{\cos(5\omega t)}{16} + \frac{5\cos(3\omega t)}{16} \right) + \left( 96a^6\beta_6 + 112a^3\beta_4 \right) \left( \frac{\cos(4\omega t)}{8} + \frac{\cos(2\omega t)}{2} + \frac{3}{8} \right) \right) + \\ & \left( 175a^5\beta_5 + 210a^3\beta_3 \right) \left( \frac{\cos(3\omega t)}{4} + \frac{3\cos(\omega t)}{4} \right) + \\ & \left( 384a^6\beta_6 + 420a^4\beta_4 + 28a^3\beta_4 + 560a^2\beta_2 \right) \left( \frac{\cos(2\omega t)}{2} + \frac{1}{2} \right) + \\ & \left( 240a^6\beta_6 - 245a^5\beta_5 + 420a^4\beta_4 + (-210\beta_3 - 84\beta_4)a^3 + 560a^2\beta_2 + 1680\beta_0 \right) \cos(\omega t) - \\ & \left( 768a^6\beta_6 - 840a^4\beta_4 - 56a^3\beta_4 - 1120a^2\beta_2 - 1680\beta_0 \right) \end{aligned} \right) \\ * \left( \begin{aligned} & \cosh\left(\frac{\beta x}{l}\right) - \cos\left(\frac{\beta x}{l}\right) - \\ & \frac{\sinh(\beta) + \sin(\beta)}{\cosh(\beta) + \cos(\beta)} \left( \sinh\left(\frac{\beta x}{l}\right) - \sin\left(\frac{\beta x}{l}\right) \right) \end{aligned} \right) \quad (57)$$

## 4. Results and Discussion

The scientific analysis of the simulated outcome using the answers found in chapter three is the main topic of this part.

### 4.1. Buckled Dynamic Shape Function of the SWCNT's

Figures 2, 3, 4, and 5 illustrate how Casimir force is affected by the dynamic response analysis of single-wall carbon nanotubes in a temperature, magnetic, and electrostatic environment. Indicating the structure's propensity to deform at particular natural frequencies, they exhibit deflections at five different buckling and mode forms.

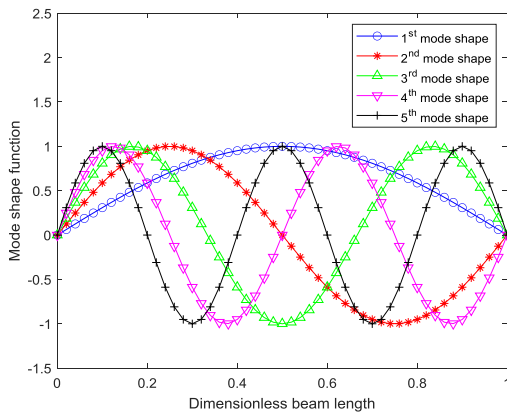


**Figure 2.** Pinned-pinned supports, illustrating mode number effects on mode form.

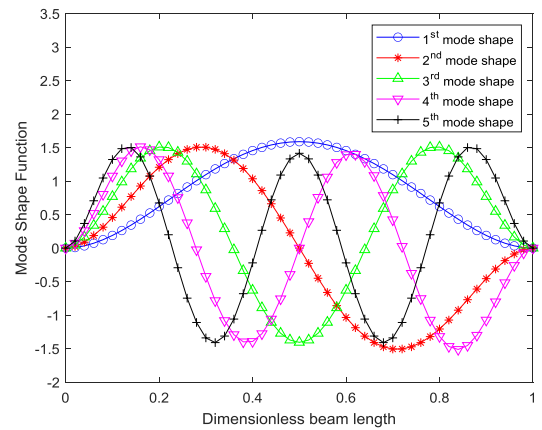


**Figure 3.** Clamped-clamped supports, illustrating mode number effects on mode form.

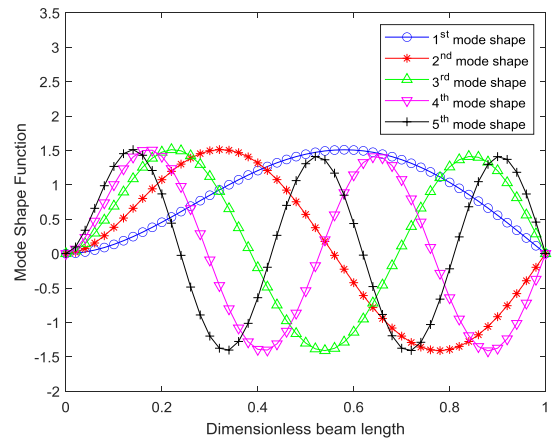


**Figure 4.** Clamped-pinned supports, illustrating mode number effects on mode form.

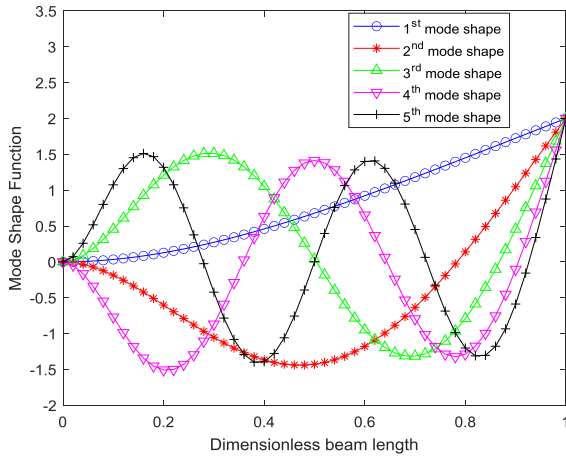


**Figure 5.** Clamped-free supports illustrating mode number effects on mode form.

## 4.2. Single-Walled Carbon Nanotube (SWCNT) Stability Response

### 4.2.1. Displaying Effects of Different Thermal Parameter on SWCNT's Stability Responses

Figures 6, 7, 8, and 9 illustrate how the thermal term of various end conditions affects the dimensionless amplitude-frequency ratio curve of the dynamic response analysis of single-wall carbon nanotubes with surface effect and geometric imperfection that are supported by elastic foundations in a thermal-magnetic-electrostatic environment while being affected by Casimir force. On the other hand, Figure 9 shows that the rise from zero to maximum frequency response reduces as well, even if the thermal term grows from zero to maximum frequency response above linear system. These demonstrate that in order to stabilize the structure of SWCNTs, the thermal term in Figures 6, 7, and 8 must be maintained at their minimums, while the thermal term in Figure 9 must be maintained at its maximum.

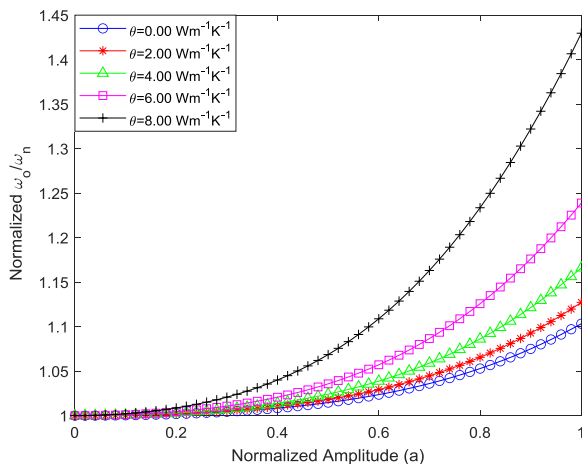


**Figure 6.** Illustrating thermal influencing stability response on SWCNT pinned-pinned supports.

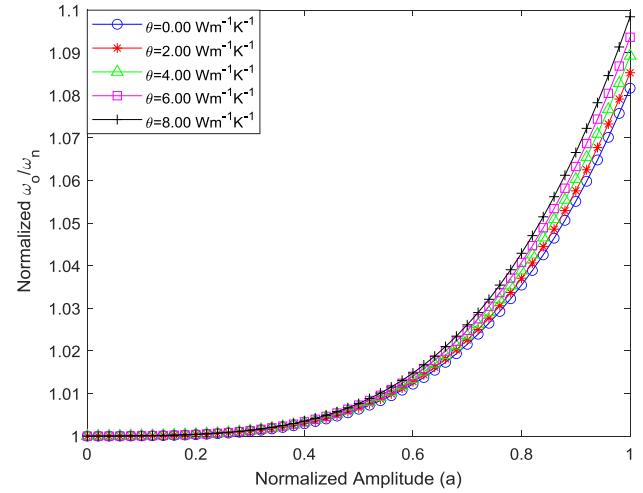


**Figure 7.** Illustrating thermal influencing stability response on SWCNT clamped-clamped supports.

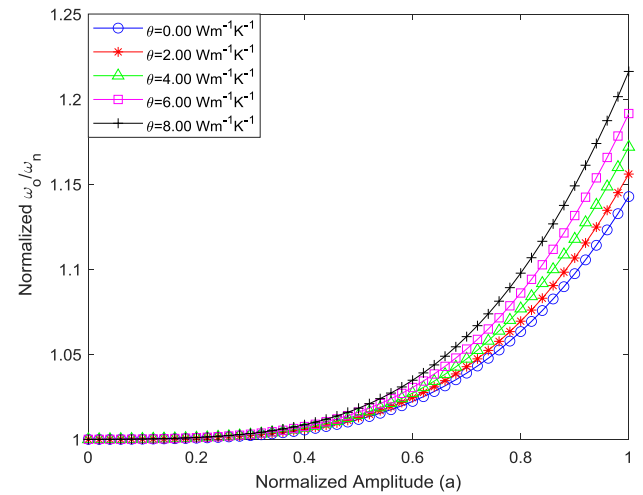


**Figure 8.** Illustrating thermal influencing stability response on SWCNT clamped-pinned supports.

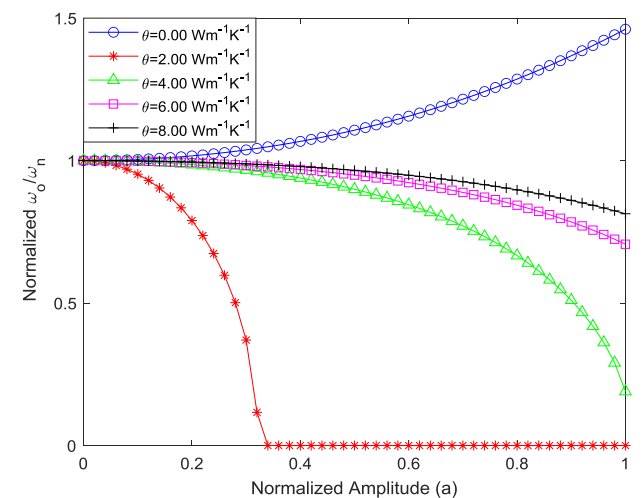


**Figure 9.** Illustrating thermal influencing stability response on SWCNT clamped-free supports.

#### 4.2.2. Displaying Effects of Different Magnetic Parameter on SWCNT's Stability Responses

Figures 10, 11, 12, and 13 illustrate how various magnetic term boundary conditions affect the dimensionless amplitude-frequency ratio curve of the dynamic response analysis of single-wall carbon nanotubes with surface effect and geometric imperfection that are supported by elastic foundations in a magneto-thermal-electrostatic environment while Casimir force is present. The figures show that the magnetic term raises the frequency response above the linear system from zero to maximum, while Figure 13 shows that the frequency response lowers as well. These demonstrate that in order to stabilize the structure of SWCNTs, the magnetic term in Figures 10, 11, and 12 must be maintained at both minimums, whereas the magnetic term in Figure 13 must be maintained at its maximum.

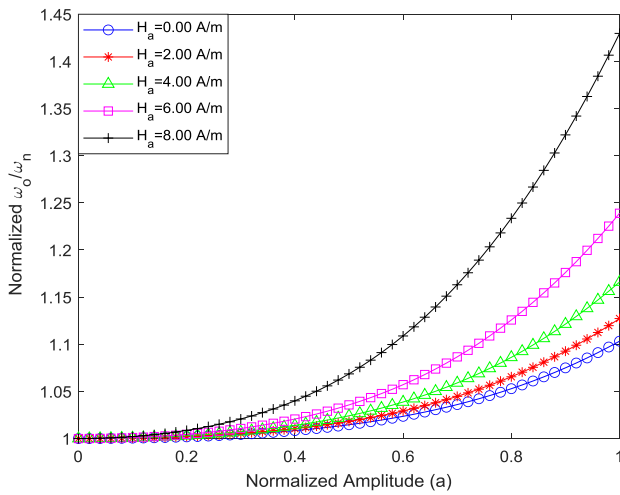


Figure 10. Illustrating magnetic influencing stability response on SWCNT pinned-pinned supports.

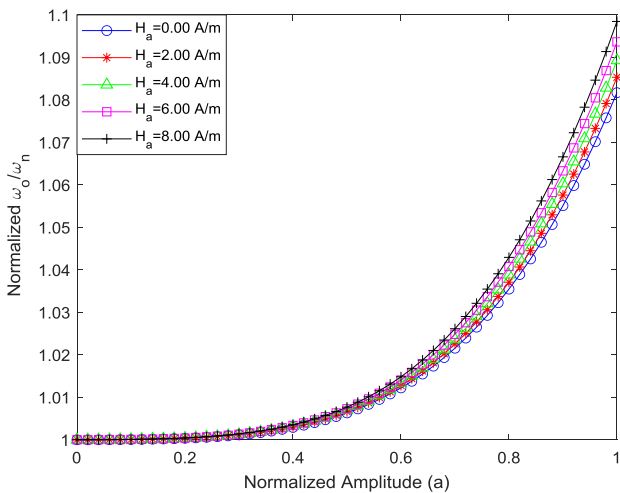


Figure 11. Illustrating magnetic influencing stability response on SWCNT clamped-clamped supports.

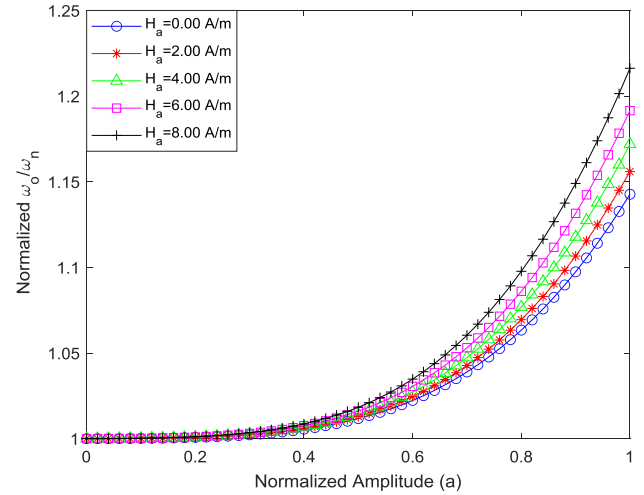


Figure 12. Illustrating magnetic influencing stability response on SWCNT clamped-pinned supports.

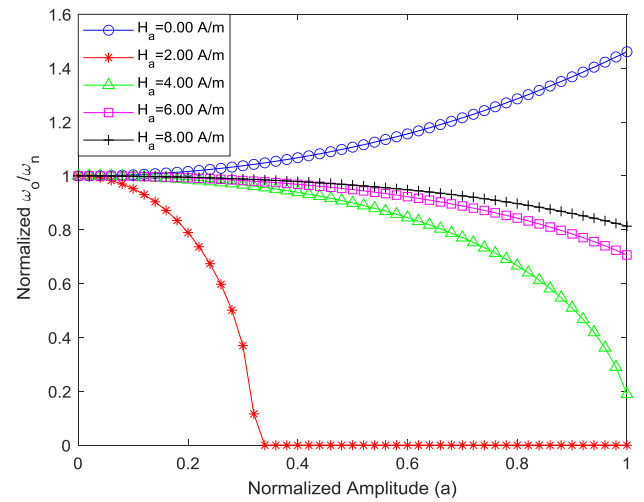
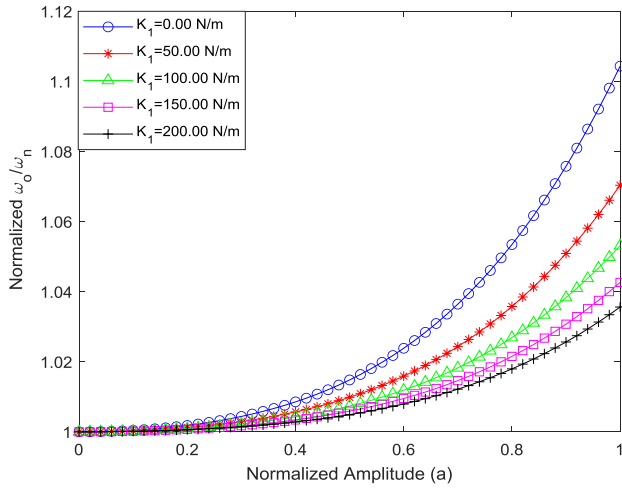


Figure 13. Illustrating magnetic influencing stability response on SWCNT clamped-free supports.

#### 4.2.3. Displaying Effects of Different Linear Foundation on SWCNT's Stability Responses

Figures 14, 15, 16, and 17 illustrate how various boundary conditions of the linear Winkler elastic foundation affect the dimensionless amplitude-frequency ratio curve of the dynamic response analysis of single-wall carbon nanotubes with surface effect and geometric imperfection resting on elastic foundations in a magneto-thermal-electrostatic environment while being affected by Casimir force. Nevertheless, the data show that the frequency-ratio falls toward a linear system as the linear Winkler elastic medium grows from zero to maximum, indicating that the structure must be maintained at maximum in order to acquire stability. Furthermore, because clamped-free foundations are becoming more linear, they are a better choice for this kind of building.



**Figure 14.** Linear foundation influencing stability response on SWCNT pinned-pinned.

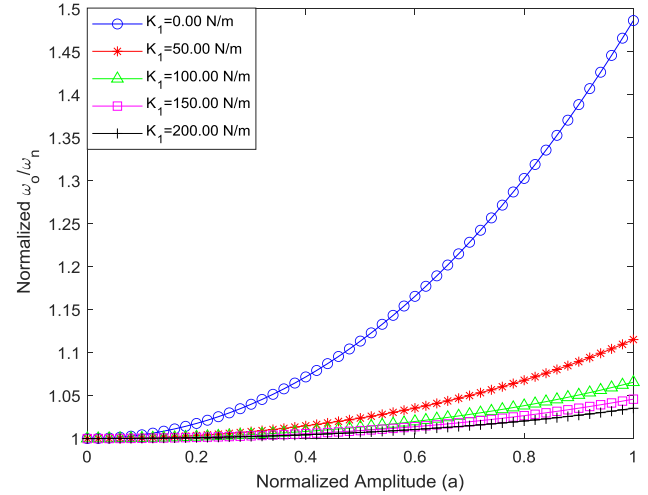


**Figure 17.** Linear foundation influencing stability response on SWCNT clamped-free.

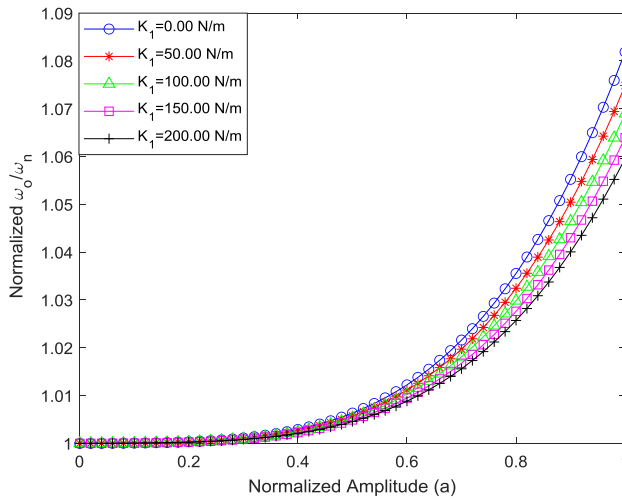


**Figure 15.** Linear foundation influencing stability response on SWCNT clamped-clamped.

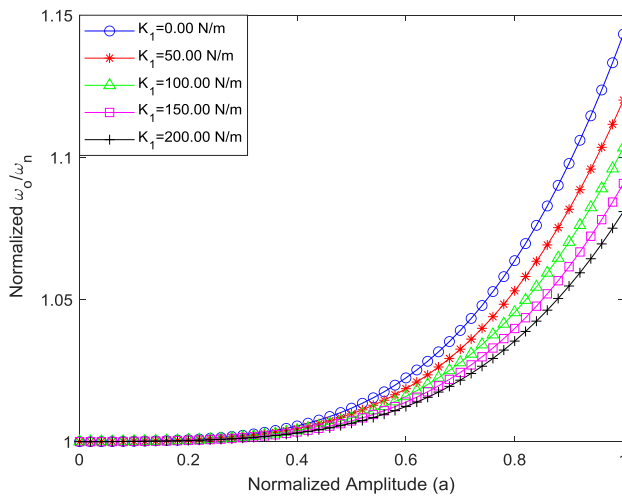


**Figure 16.** Linear foundation influencing stability response on SWCNT clamped-pinned.

#### 4.2.4. Displaying Effects of Different Pasternak Foundation on SWCNT's Stability Responses

Figures 18, 19, 20, and 21 illustrate how the Pasternak elastic medium with various boundary conditions affects the dynamic response analysis's dimensionless amplitude-frequency ratio curve for single-wall carbon nanotubes with surface effect and geometric imperfection that are supported by elastic foundations in a magneto-thermal-electrostatic environment while being affected by Casimir force. As seen in Figures 18, 19, and 20, the Pasternak elastic medium grows from zero to maximum frequency response, surpassing the linear system. However, Figure 21 shows a drop in frequency response as well. These demonstrate that in order to stabilize the structure of SWCNTs, the Pasternak foundation for Figures 18, 19, and 20 must be maintained at both minimum and maximum, but Figure 21's foundation must be maintained at maximum.

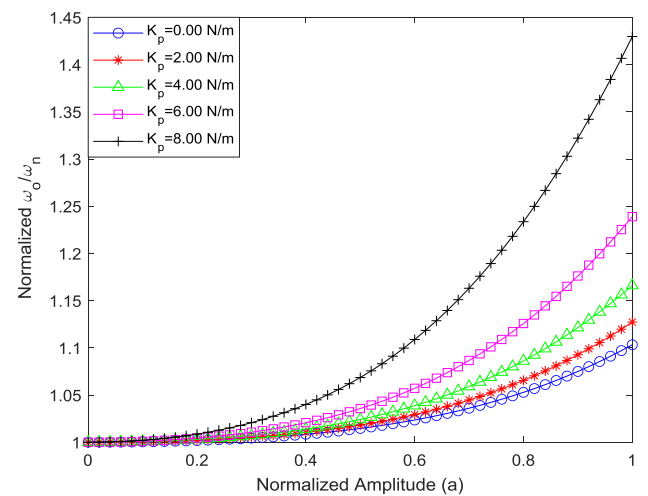


**Figure 18.** Pasternak foundation influencing stability response on SWCNT pinned-pinned.



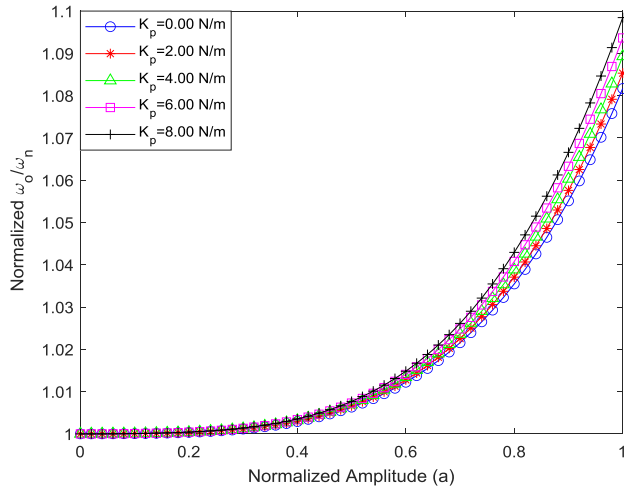


**Figure 19.** Pasternak foundation influencing stability response on SWCNT clamped-clamped.

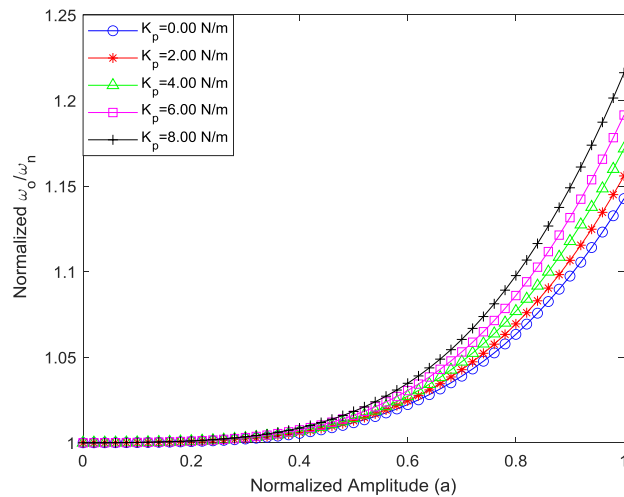


**Figure 20.** Pasternak foundation influencing stability response on SWCNT clamped-pinned.

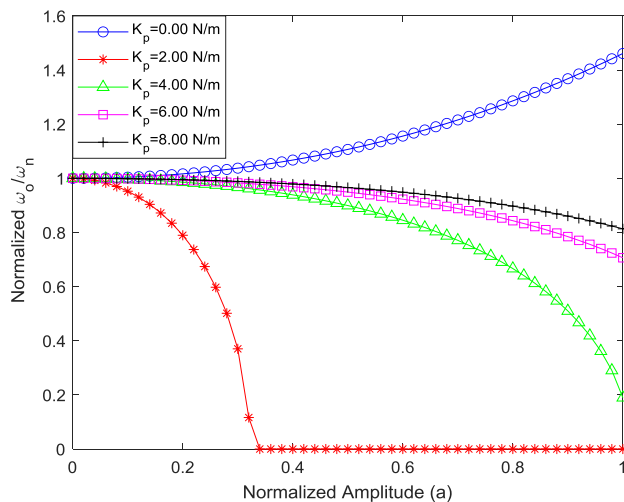


**Figure 21.** Pasternak foundation influencing stability response on SWCNT clamped-free.

#### 4.2.5. Displaying Effects of Different Nonlinear Foundation on SWCNT's Stability Responses

The impact of various boundary conditions of the nonlinear Winkler elastic medium on the dimensionless amplitude-frequency ratio curve of vibration of single-walled carbon nanotubes resting on an elastic foundation with thermal and magnetic effects under the influence of electrostatic force is depicted in Figures 22, 23, 24, and 25. Figures 22, 23, 24, and 25 show that the frequency-ratio grows in proportion to the nonlinear Winkler-type elastic medium's growth from zero to maximum. This demonstrates that a minimal nonlinear Winkler elastic basis is required for the structure of SWCNTs to become stable.

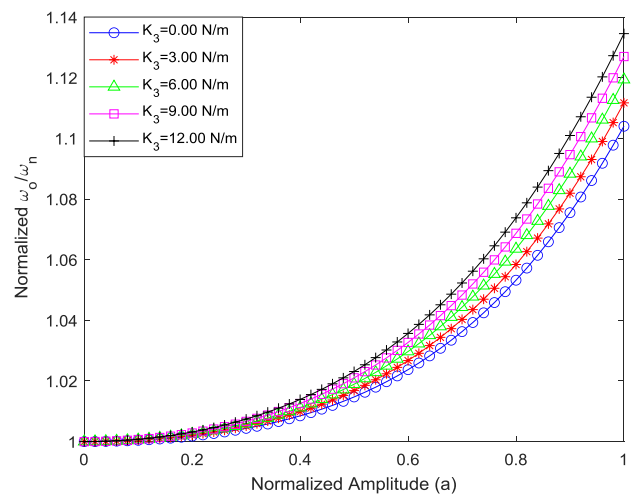


**Figure 22.** Nonlinear foundation influencing stability response on SWCNT pinned-pinned.

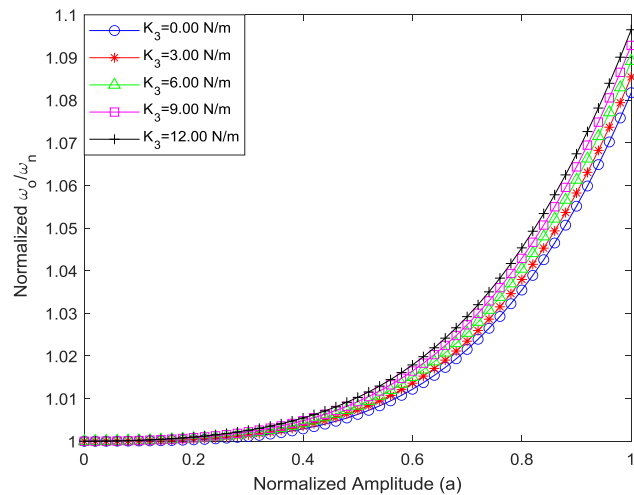


**Figure 23.** Nonlinear foundation influencing stability response on SWCNT clamped-clamped.

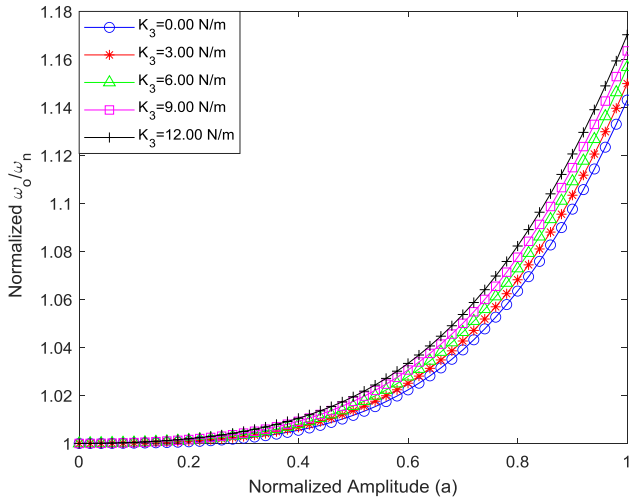


**Figure 24.** Nonlinear foundation influencing stability response on SWCNT clamped-pinned.

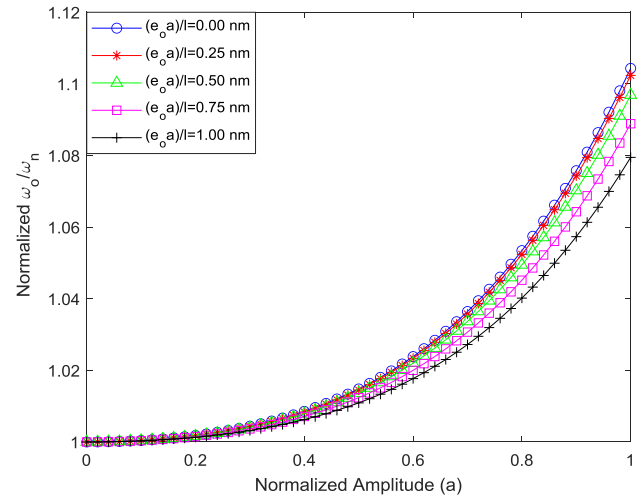


**Figure 26.** Nonlocal parameter influencing stability response on SWCNT pinned-pinned.

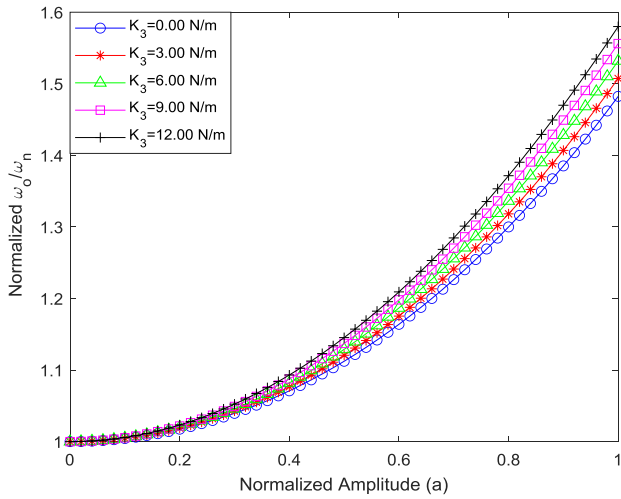


**Figure 25.** Nonlinear foundation influencing stability response on SWCNT clamped-free.

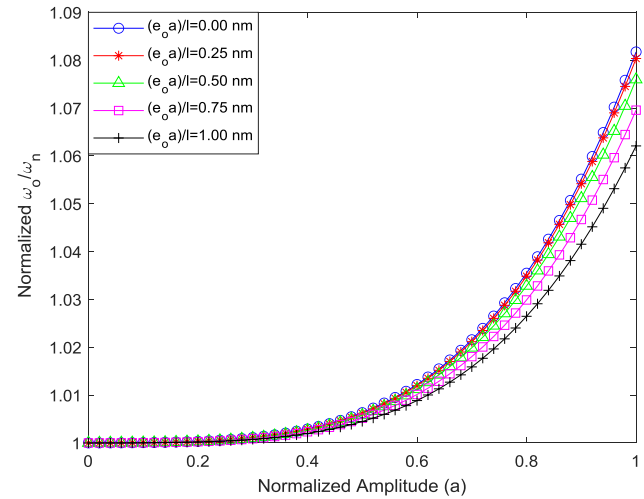


**Figure 27.** Nonlocal parameter influencing stability response on SWCNT clamped-clamped.

#### 4.2.6. Displaying Effects of Nonlocal Parameter on SWCNT's Stability Responses

Under the influence of electrostatic force, Figures 26, 27, 28, and 29 illustrate how the nonlocal parameter of various boundary conditions affects the dimensionless amplitude-frequency ratio curve of vibration of single-walled carbon nanotubes resting on an elastic foundation with magnetic and thermal effects. When seen in Figures 26, 27, 28, and 29, the frequency-ratio also falls when the nonlocal parameter rises from zero to maximum. Nevertheless, in order to ensure stability for all of the end circumstances taken into account during simulations, the nonlocal value should be kept as low as possible.

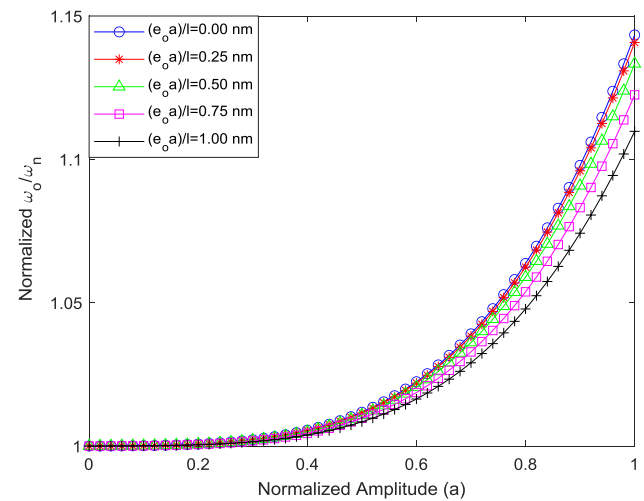


**Figure 28.** Nonlocal parameter influencing stability response on SWCNT clamped-pinned.

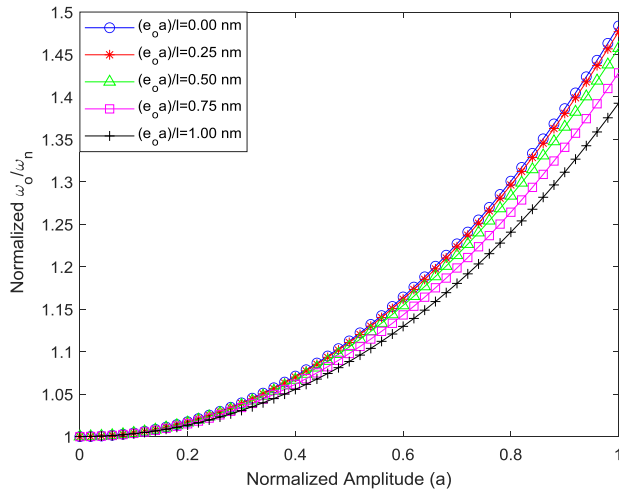


**Figure 29.** Nonlocal parameter influencing stability response on SWCNT clamped-free.

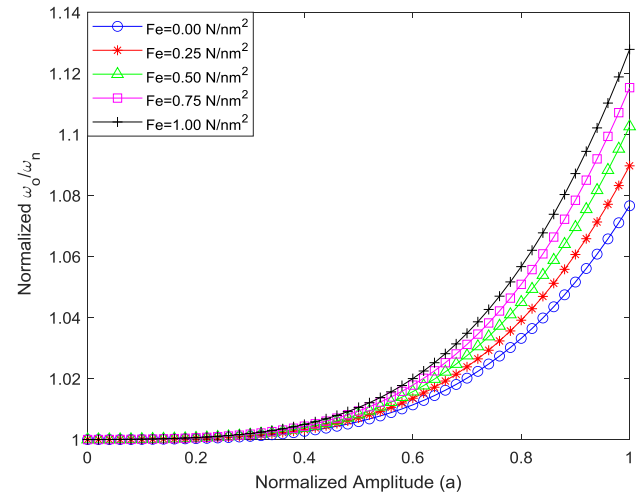


**Figure 31.** Electrostatic force influencing stability response on SWCNT clamped-clamped.

#### 4.2.7. Displaying Effects of Different Electrostatic Force on SWCNT's Stability Responses

Under the influence of Casimir force, Figures 30, 31, 32, and 33 illustrate how the electrostatic force of various boundary conditions affects the dimensionless amplitude-frequency ratio curve of the dynamic response analysis of single-wall carbon nanotubes with surface effect and geometric imperfection resting on elastic foundations in a magneto-thermal-electrostatic environment. According to the numbers, the frequency-ratio increases as electrostatic force grows from zero to maximum. However, in order to establish stability, the electrostatic force should be reduced to a minimum.

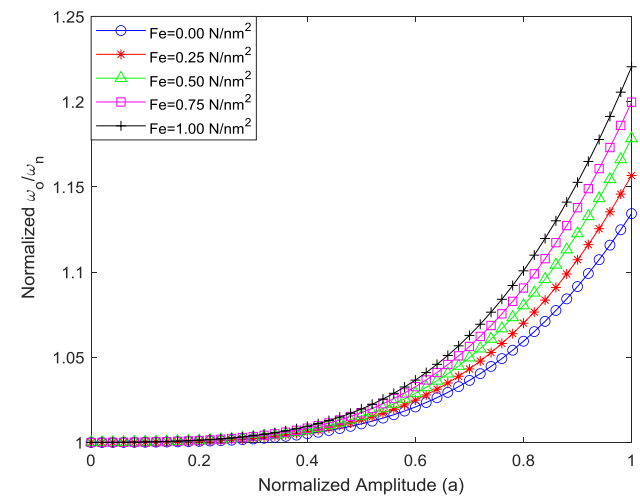


**Figure 32.** Electrostatic force influencing stability response on SWCNT clamped-pinned.

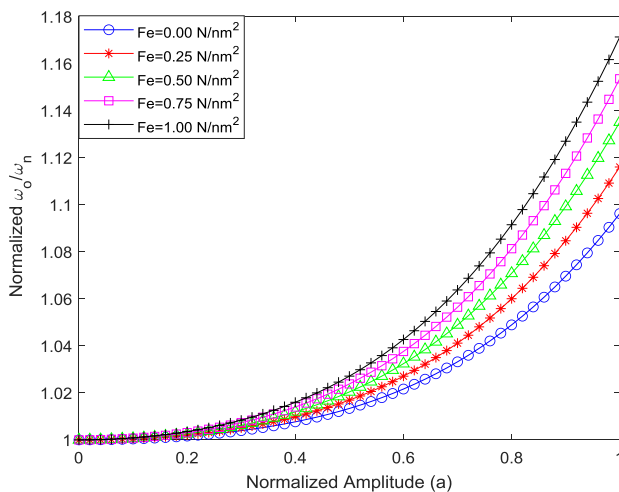


**Figure 30.** Electrostatic force influencing stability response on SWCNT pinned-pinned.

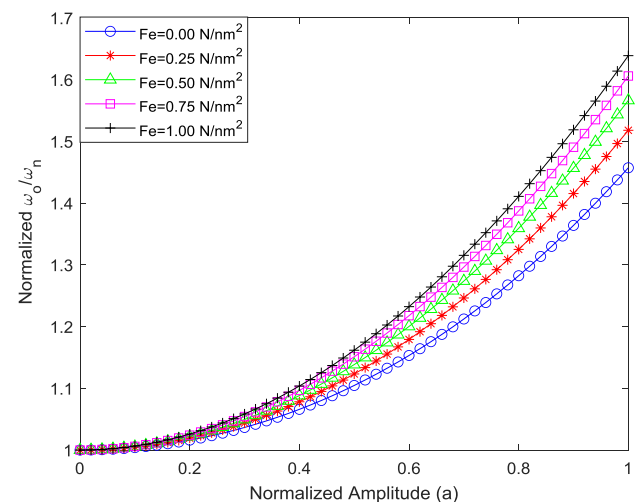


**Figure 33.** Electrostatic force influencing stability response on SWCNT clamped-free.

#### 4.2.8. Displaying Effects of Different Van der Waals Force on SWCNT's Stability Responses

Van der Waals force of various boundary conditions is shown to have an impact on the dimensionless amplitude-frequency ratio curve of dynamic response analysis of single-wall carbon nanotubes with surface effect and geometric imperfection resting on elastic foundations in a magneto-thermal-electrostatic environment under the influence of Casimir force in Figures 34, 35, 36, and 37. According to the numbers, the frequency-ratio rises as the van der Waal force grows from zero to maximum. Nonetheless, to maintain stability, the van der Waals force should be minimized.

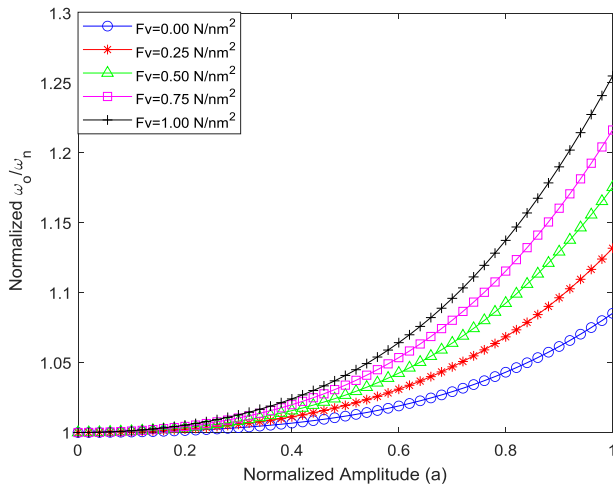


**Figure 34.** Van der Waals force influencing stability response on SWCNT pinned-pinned.

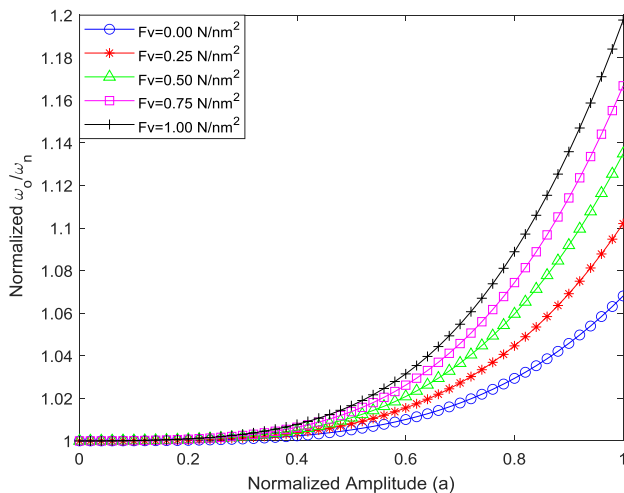


**Figure 35** Van der Waals force influencing stability response on SWCNT clamped-clamped.

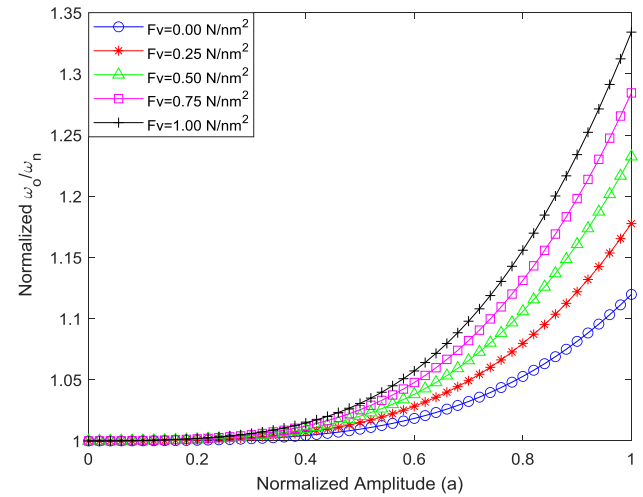


**Figure 36.** Van der Waals force influencing stability response on SWCNT clamped-pinned.

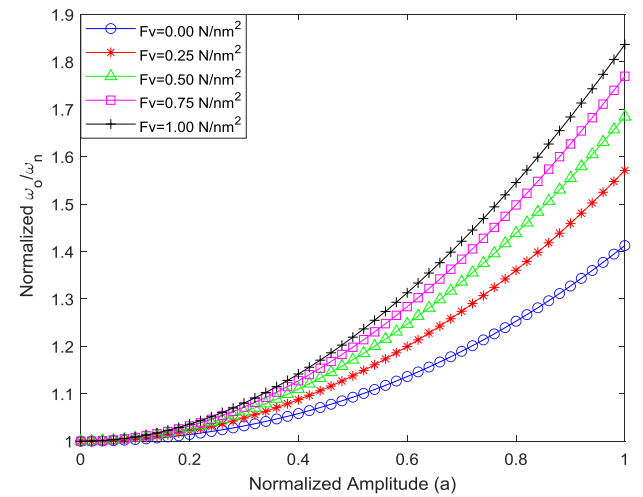


**Figure 37.** Van der Waals force influencing stability response on SWCNT clamped-free.

#### 4.2.9. Displaying Effects of Different Casimir Force on SWCNT's Stability Responses

In the dynamic response analysis of single-wall carbon nanotubes with surface effect and geometric imperfection resting on elastic foundations in a magneto-thermal-electrostatic environment, the effect of different boundary conditions' Casimir forces on the dimensionless amplitude-frequency ratio curve is seen in Figures 38, 39, 40, and 41. The data show that the frequency-ratio grows as the Casimir force rises from zero to maximum. To maintain stability, the Casimir force should be minimized in this way.

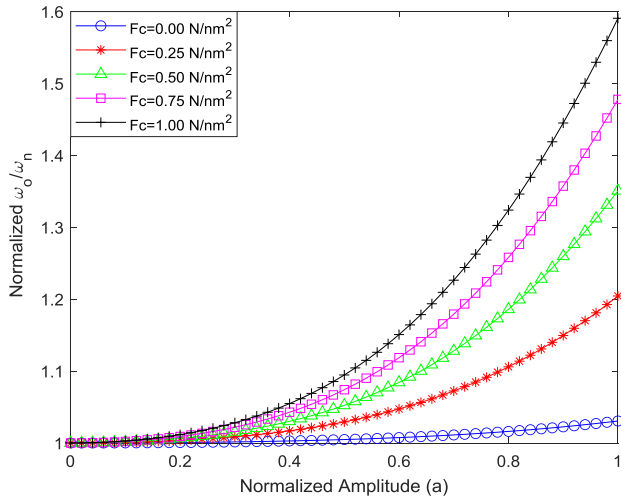


**Figure 38.** Casimir force influencing stability response on SWCNT pinned-pinned.

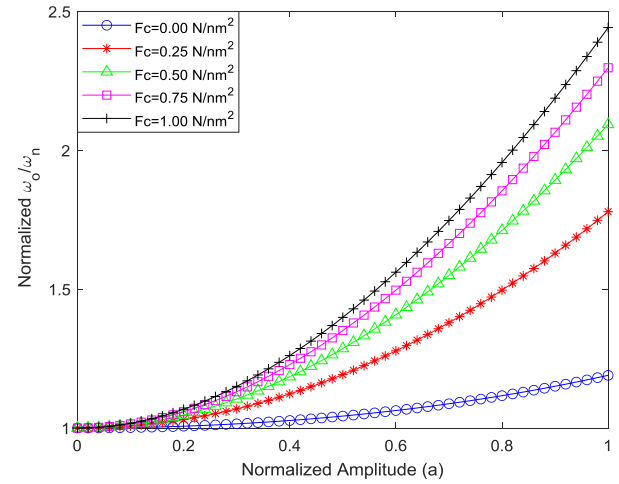


**Figure 41.** Casimir force influencing stability response on SWCNT clamped-free.

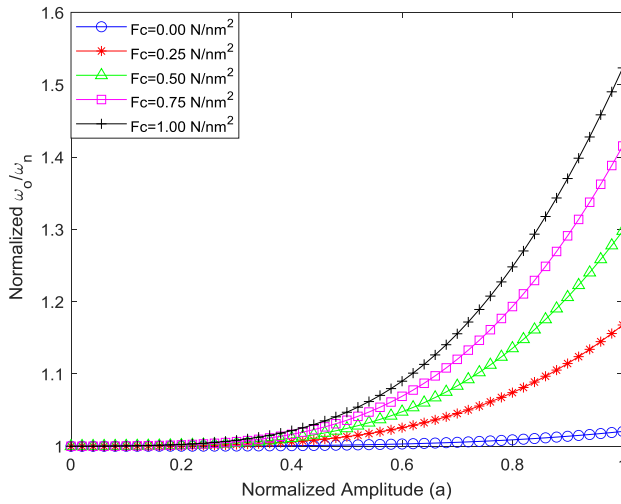


**Figure 39.** Casimir force influencing stability response on SWCNT clamped-clamped.

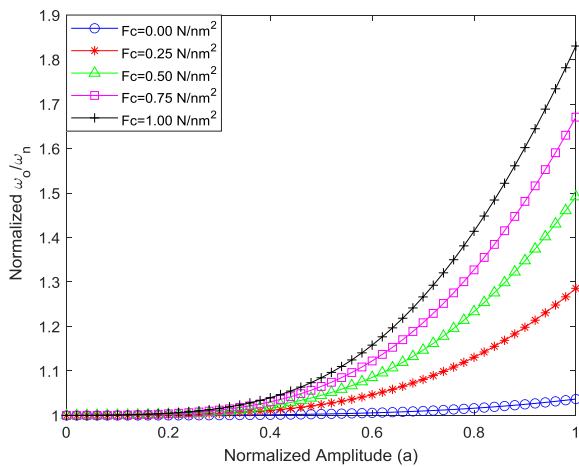


**Figure 40.** Casimir force influencing stability response on SWCNT clamped-pinned.

### 4.3. Single-Walled Carbon Nanotube Stability Response on Boundary Conditions

#### 4.3.1. Displaying Effects of Four ends Supports on SWCNT's Stability Responses

The dynamic response analysis of single-wall carbon nanotubes with geometric imperfections resting on elastic foundations in a magneto-thermal-electrostatic environment under the influence of Casimir force is shown in **Figure 42**, where the impact of four boundary conditions is depicted. The maximum frequency ratio is shown by clamped-free, clamped-pinned, and pinned-pinned supports. The lowest frequency ratio, however, is seen in clamped-clamped support. Because of this, it is possible to manage the stability of any elastic foundation when a system is subjected to Casimir force by using clamped-clamped support, which exhibits the best foundation types with the lowest frequency ratio.

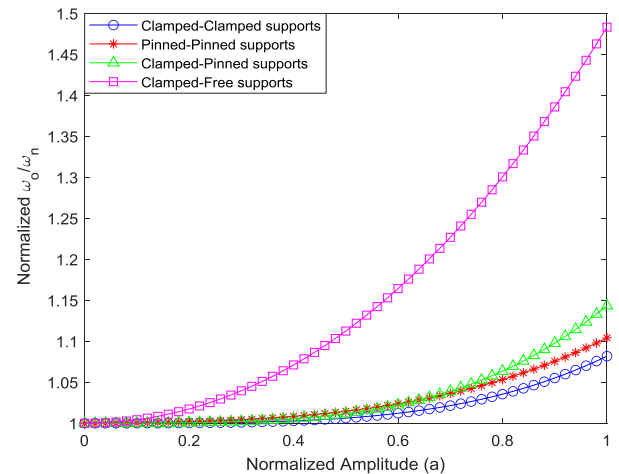


**Figure 42.** Illustrating how four different boundary conditions affects SWCNT stability response.

#### 4.3.2. Displaying Effects of Three Ends Supports on SWCNT's Stability Responses

The dynamic response analysis of single-wall carbon nanotubes with geometric imperfections resting on elastic foundations in a magneto-thermal-electrostatic environment under the influence of Casimir force is shown in Figure 44, where the impact of two boundary conditions is depicted. The maximum frequency ratio is shown by clamped-free, clamped-pinned, and pinned-pinned supports in Figure 44. The lowest frequency ratio, however, is seen in clamped-clamped support. Because of this, it is possible to manage the stability of any elastic foundation when a system is subjected to Casimir force by using clamped-clamped support, which exhibits the best foundation types with the lowest frequency ratio.

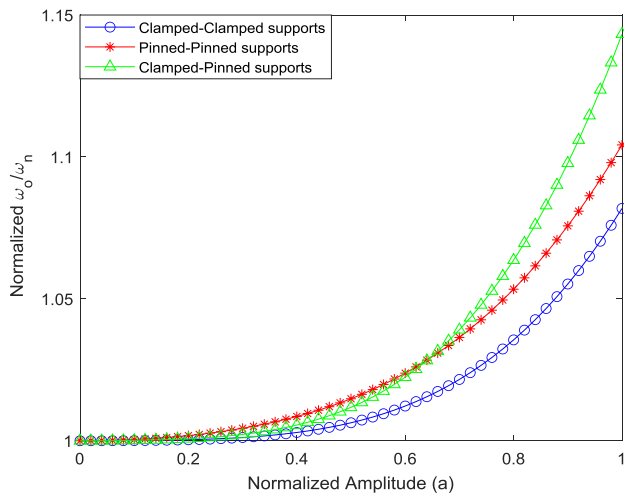


**Figure 43.** Illustrating how three different boundary conditions affects SWCNT stability response.

The dynamic response analysis of single-wall carbon nanotubes with geometric imperfections resting on elastic foundations in a magneto-thermal-electrostatic environment under the influence of Casimir force is shown in Figure 43, where the impact of three boundary conditions is depicted. The maximum frequency ratio is shown by clamped-free, clamped-pinned, and pinned-pinned supports in Figure 43. The lowest frequency ratio, however, is seen in clamped-clamped support. Because of this, it is possible to manage the stability of any elastic foundation when a system is subjected to Casimir force by using clamped-clamped support, which exhibits the best foundation types with the lowest frequency ratio.

#### 4.3.3. Displaying Effects of Two Ends Supports on SWCNT's Stability Responses

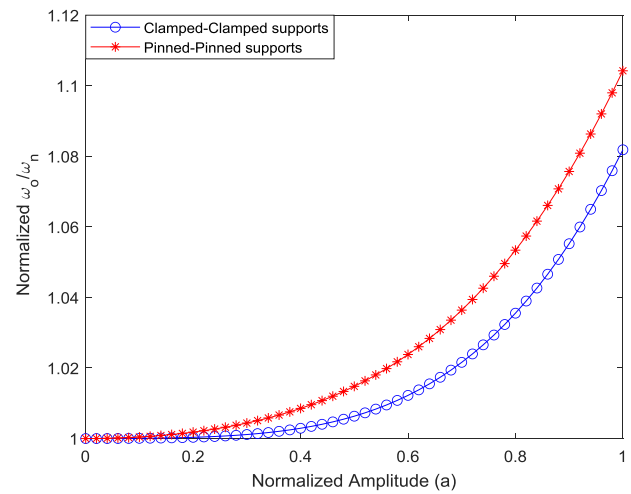


**Figure 44.** Illustrating how two different boundary conditions affects SWCNT stability response.

#### 4.3.4. Displaying Effects of One End Supports on SWCNT's Stability Responses

The dynamic response analysis of single-wall carbon nanotubes with geometric imperfections resting on elastic foundations in a magneto-thermal-electrostatic environment under the influence of Casimir force is shown in Figure 45, where the impact of one boundary conditions is depicted. The maximum frequency ratio is shown by clamped-clamped. The stability of any elastic foundation can be managed when a system is subjected to Casimir force by using clamped-clamped support, which exhibits the best foundation type.

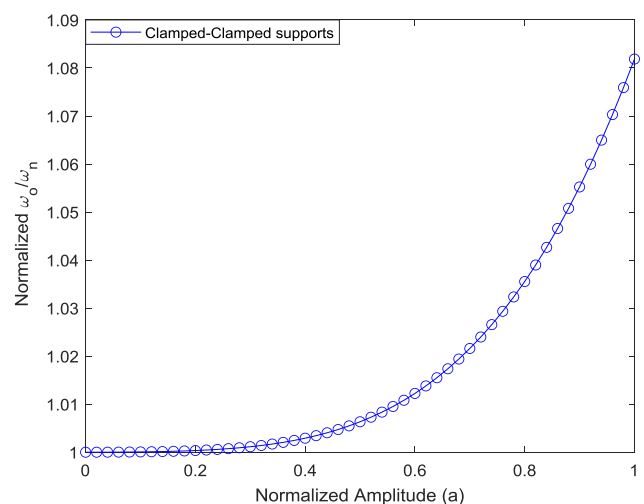


**Figure 45.** Illustrating how one different boundary condition affects SWCNT stability response.



## 4.4. Single-Walled Carbon Nanotube's Dynamic Responses

### 4.4.1. Displaying Impacts of Different Casimir Force on SWCNT's Dynamic Responses

A dynamic response study of single-wall carbon nanotubes with geometric imperfections lying on elastic foundations in a magneto-thermal-electrostatic environment under the effect of Casimir force is shown in Figures 46, 47, 48, and 49. The time-deflection curve's deflection across each end supports the corresponding decrease towards the crest as the Casimir force grows from zero to maximum. Therefore, when the forces grow from zero to maximum in the case of clamped-free supports, the deflection trough changes into a deflection crest after the first two simulations.

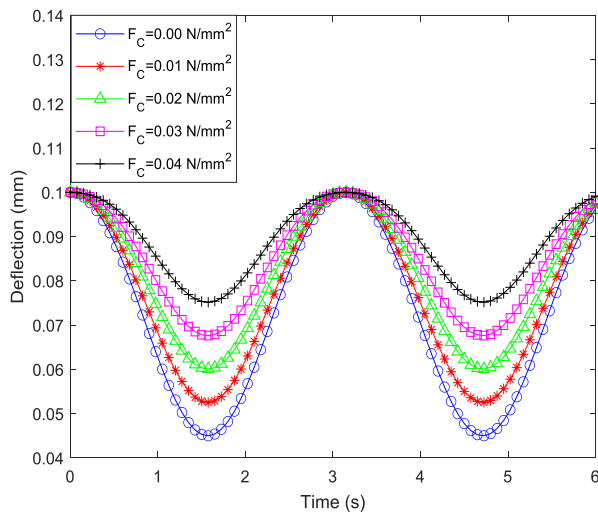


**Figure 46.** Casimir force influencing dynamic response on SWCNT pinned-pinned supports.

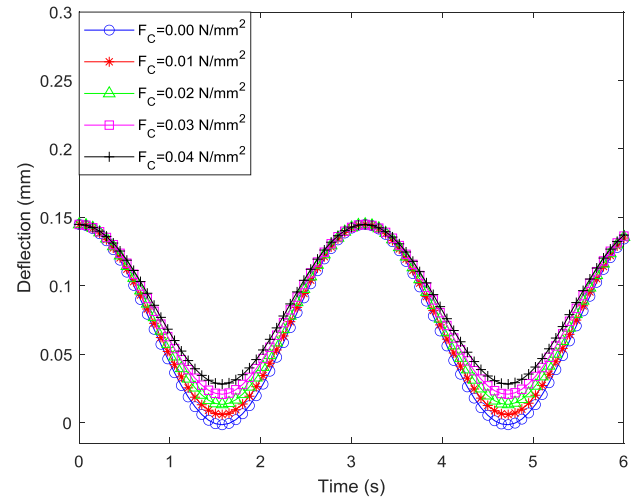


**Figure 48.** Casimir force influencing dynamic response on SWCNT clamped-pinned supports.

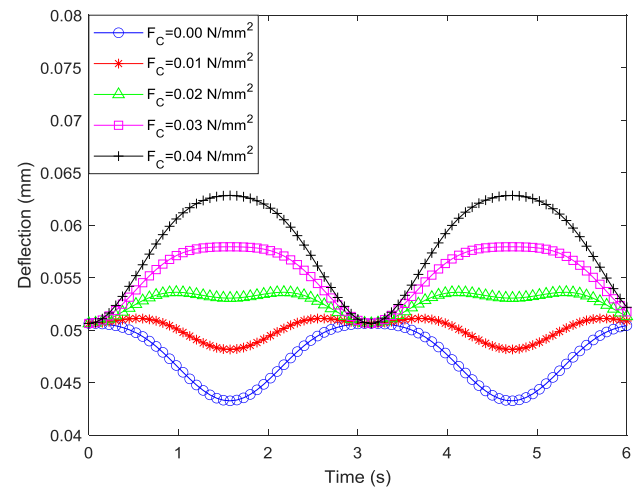


**Figure 49.** Casimir force influencing dynamic response on SWCNT pinned-free supports.

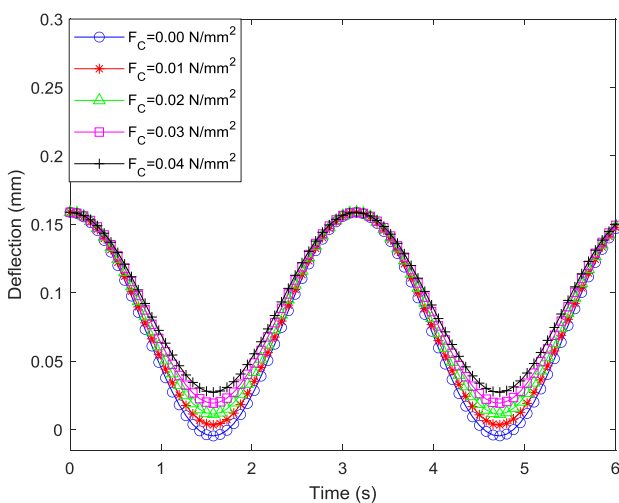


**Figure 47.** Casimir force influencing dynamic response on SWCNT clamped-clamped supports.

### 4.4.2 Displaying Impacts of Different Van der Waals Force on SWCNT's Dynamic Responses

Van der Waal force has an impact on the time-deflection curve of the dynamic response analysis of single-wall carbon nanotubes with geometric imperfections resting on elastic foundations in a magneto-thermal-electrostatic environment under the influence of Casimir force, as shown in Figures 50, 51, 52, and 53. As van der Waal force increases from zero to maximum, the deflection trough of the time-deflection curve for each end support considered decreases towards the crest, so that in the case of clamped-free supports, following the first two simulations, the deflection trough changes into the deflection crest.

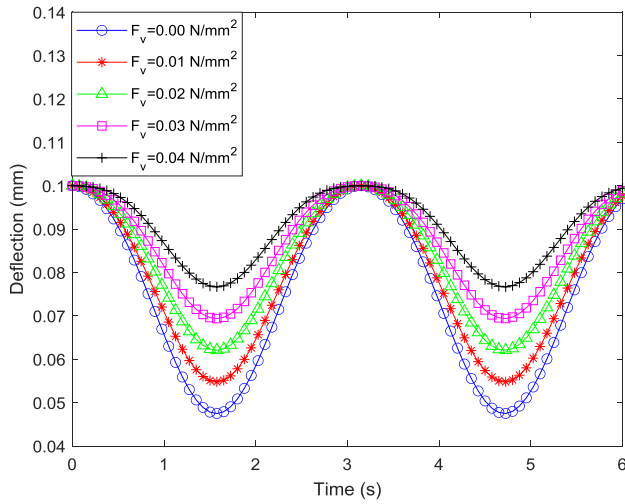


**Figure 50.** Van der Waals force influencing dynamic response SWCNT pinned-pinned.

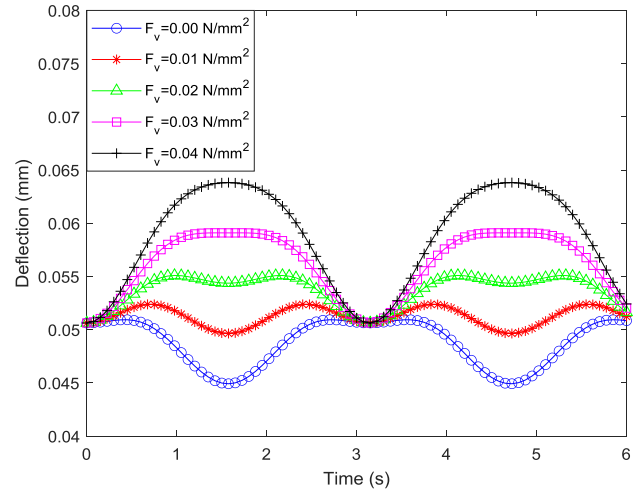


**Figure 53.** Van der Waals force influencing dynamic response SWCNT clamped-free.

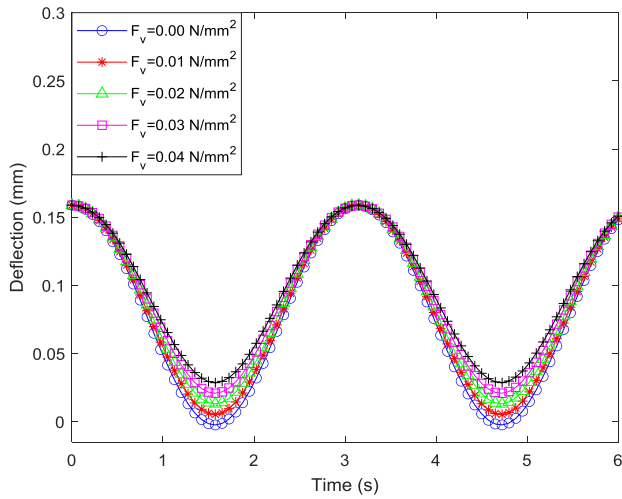


**Figure 51.** Van der Waals force influencing dynamic response SWCNT clamped-clamped.

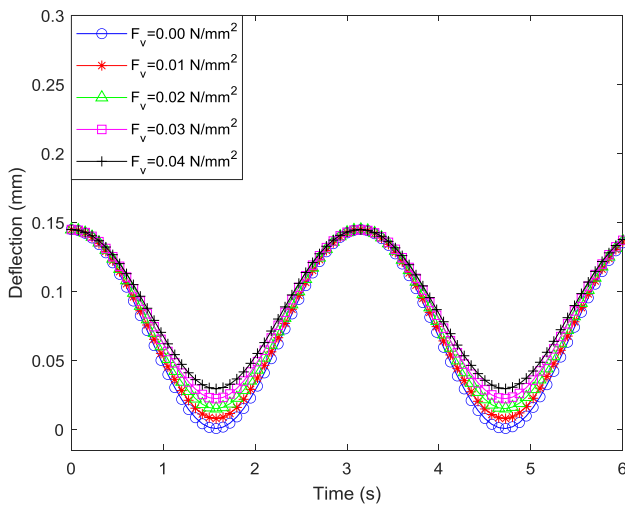


**Figure 52.** Van der Waals force influencing dynamic response SWCNT clamped-pinned.

#### 4.4.3 Displaying Impacts of Different Electrostatic Force on SWCNT's Dynamic Responses

Electrostatic force's effect on the time-deflection curve of the dynamic response analysis of single-wall carbon nanotubes with geometric imperfections resting on elastic foundations in a magneto-thermal-electrostatic environment under the influence of Casimir force is depicted in Figures 54, 55, 56, and 57. The deflection trough of the time-deflection curve for either end supports the corresponding drop towards the crest as electrostatic force grows from zero to maximum. As the forces grow from zero to maximum, the deflection trough in the case of clamped-free supports changes to a deflection crest after the first two simulations.

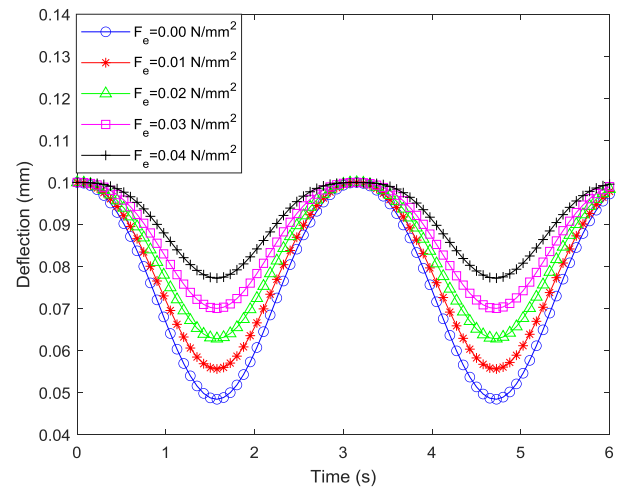


**Figure 54.** Electrostatic force influencing dynamic response SWCNT pinned-pinned supports.



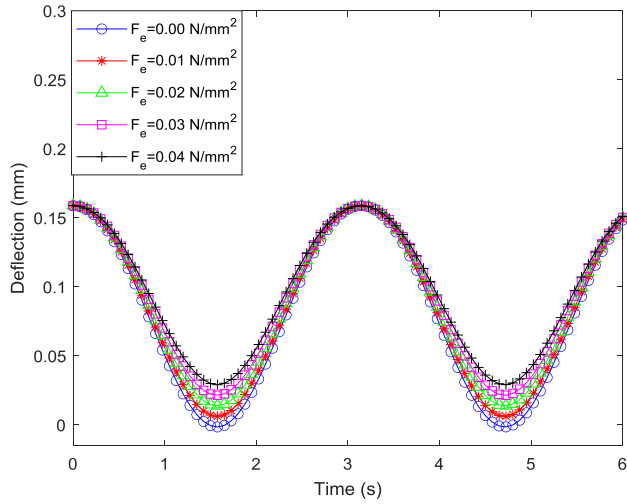


**Figure 55.** Electrostatic force influencing dynamic response SWCNT clamped-clamped supports.

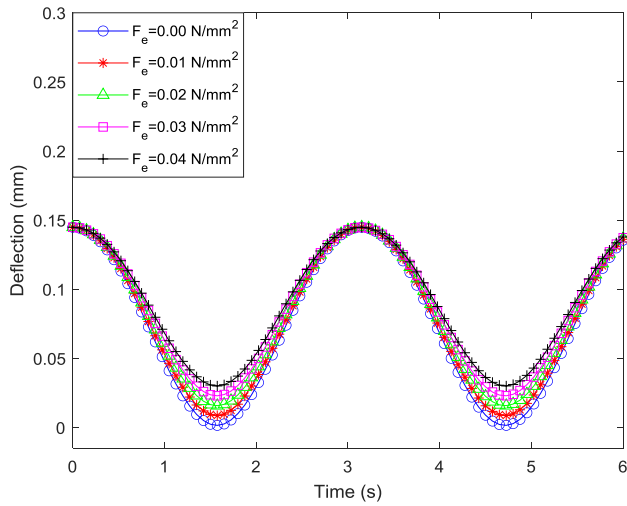


**Figure 56** Electrostatic force influencing dynamic response SWCNT clamped-pinned supports.

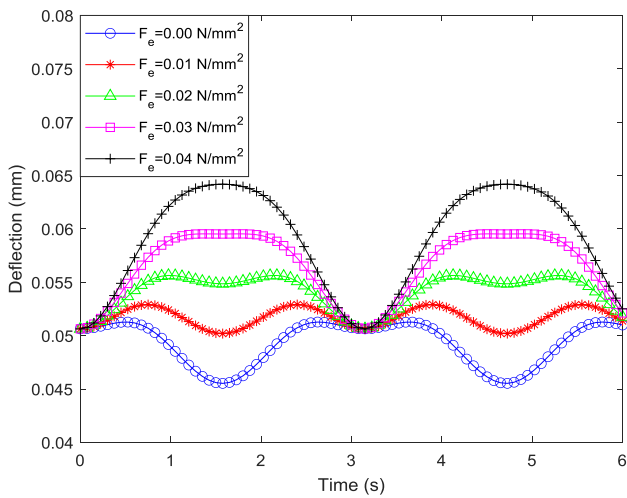


**Figure 57.** Electrostatic force influencing dynamic response SWCNT clamped-free supports.

#### 4.4.4. Displaying Impacts of Different Mass on SWCNT's Dynamic Responses

In a magneto-thermal-electrostatic environment with Casimir force acting on single-wall carbon nanotubes with geometric imperfections resting on elastic foundations, [Figures 59, 59, 60, and 61](#) illustrate how the mass of the nanotube affects the time-deflection curve of the dynamic response analysis. As mass of nanotube increases from 0.10kg to maximum, deflection crest of time-deflection curve for each ends supports considered decrease respectively towards trough. Again, when the mass of nanotube increases from minimum to maximum, deflection crest reduces as well, indicating that as the mass increases, deflection decreases for all ends conditions studied.

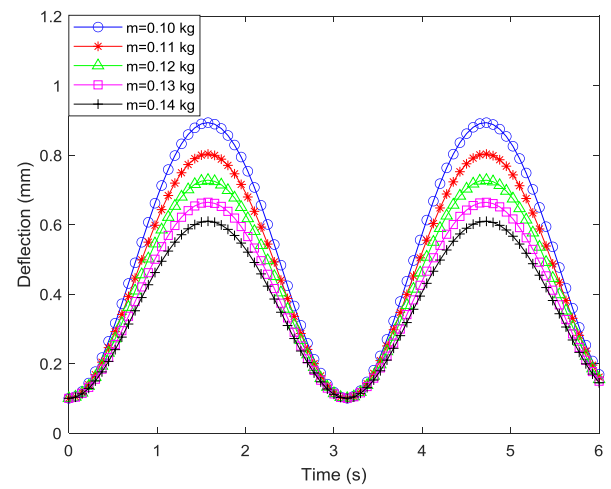


**Figure 58.** How mass affects dynamic response on pinned-pinned supports.

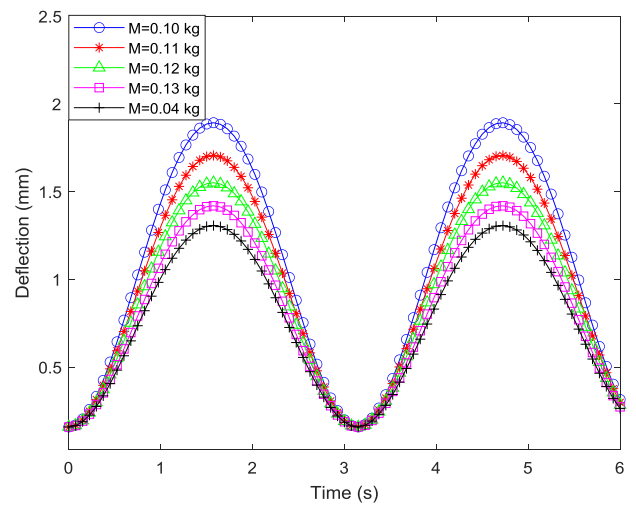


**Figure 59.** How mass affects dynamic response on clamped-clamped supports.

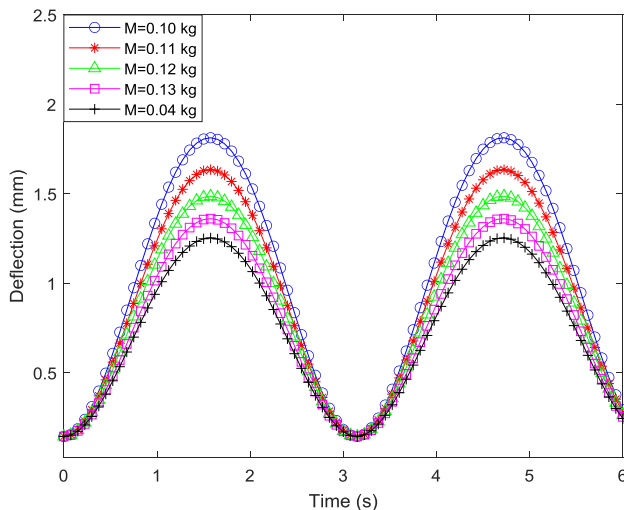


**Figure 60.** How mass affects dynamic response on clamped-pinned supports.

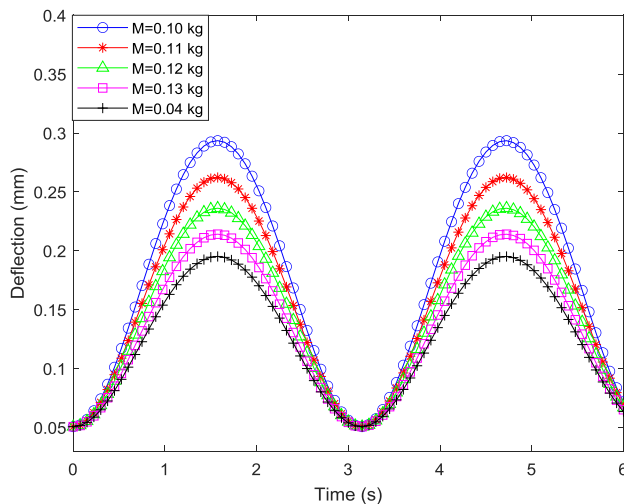


**Figure 61.** How mass affects dynamic response on clamped-free supports.

## 5. Conclusion

Using Eringen's non-local elastic theory, Euler-Bernoulli elastic beam theory, and the Hamilton principle as a basis, this work examines the nonlinear vibration analysis of single-wall carbon nanotubes with geometric imperfections resting on elastic foundations in a magneto-thermal-electrostatic environment under the influence of Casimir Force. The nonlinear mathematical model is solve using Iteration Perturbation Method after Galerkin decomposition method is applied directly to decomposed the system into spatial and temporal nonlinear duffing equation of motion. Again, MATLAB simulation was conducted on the analyzed solution as the results obtained shows influence of Casimir force, electrostatic force, and van der Waals force and mass of the nanotubes as synonymous as there contribute significantly to enhanced both compressive and tensile zones of reinforced concrete.

## Abbreviations

SWCNT	Single-Walled Carbon Nanotube
CNTs	Carbon Nanotube
SWNT	Single-Walled Nanotube
DWCNTs	Double-Walled Carbon Nanotube
PDE	Partial Differential Equation
NTRC	Nanotube Reinforcement Composites
ODE	Ordinary Differential Equation

## Conflicts of Interest

The authors declare no conflicts of interest.

## References

- [1] Abubakar, E. H., Sobamowo, M. G., Sadiq M. O., Yinusa A. A. (2023) Nonlinear Vibration Analysis of Nanotubes in A Magneto-Thermal-Electrostatic Environment under The Influence of Casimir Force, Journal of Nanomaterials and Devices, 1(1).
- [2] Anh N. D. and Hieu D. V. (2021) Nonlinear Vibration of Nonlocal Strain Gradient Nanotubes Under Longitudinal Magnetic Field, Vietnam Journal of Mechanics, Vietnam Academy of Science and Technology, 1-23, <https://doi.org/10.15625/0866-7136/15467>
- [3] Belhadj A., Boukhalfa A., Belalia S. A., (2017) Free vibration modelling of single-walled carbon nanotubes using the differential quadrature method, Mathematical Modelling of Engineering Problems, 4(1), 33-37, <https://doi.org/10.18280/mmep.040107>
- [4] E H Abubakar, M G Sobamowo, M O Sadiq, A A Yinusa (2023) Vibration of Single-walled Carbon Nanotube Resting on Elastic Foundation with Magnetic and Thermal Effects under the Influence of Casimir Force, J Nanosci Technol 1(1) 103.
- [5] Egbunu H. Abubakar, Gbeminiyi M. Sobamowo, Obanihsola M. Sadiq, Ahmed A. Yinusa (2024), Dynamic and Instability Analysis of Single Walled Carbon Nanotubes with Geometrical Imperfections Resting on Elastic Medium in a Magneto-Thermally-Electrostatic Environment with Impact of Casimir Force using Homotopy Perturbation Method, Engineering Today.
- [6] Hosseini M., Sadeghi-Goughari M., Atashipour S. A., Eftekhari M. (2014) Vibration analysis of single-walled carbon nanotubes conveying nanoflow embedded in a viscoelastic medium using modified nonlocal beam model, Arch. Mech., 66, 4, 217-244.
- [7] Matteo Strozzi, Isaac E. Elishakoff, Michele Bochicchio, Marco Cocconcelli, Riccardo Rubini 1 and Enrico Radi (2024) Nonlocal Strain Gradient Anisotropic Elastic Shell Model for Vibration Analysis of Single-Walled Carbon Nanotubes.
- [8] Mustafa Oguz Nalbant, Süleyman Murat Bağdatli, Ayla Tekin (2023), Investigation of Free Vibrations of Stepped Nanobeam Embedded in Elastic Foundation, 5th International Conference on Applied Engineering and Natural Sciences July 10-12: Konya, Turkey.

- [9] Muzamal Hussain and Muhammad Nawaz Naeem (2017), Vibration analysis of single-walled carbon nanotubes using wave propagation approach, *Mech. Sci.*, 8, 155–164.
- [10] Rafiu Olalekan Kuku, Nurudeen Adekunle Raji and Gbeminiyi Sobamowo (2024) Analytical Investigations of Thermal-Magnetic Effects on Nonlinear Vibration of Carbon Nanotube in a Multi-layer Elastic Media using Differential Transformation Method, *World Scientific News* 192, 1-21.
- [11] Ramgopal Reddy B., Ramji K. and Satyanarayana B. (2011) Free Vibration Analysis of Carbon Nanotube Reinforced Laminated Composite Panels, *International Journal of Mechanical and Mechatronics Engineering* 5(8) 1616-1620.
- [12] Ravi Kumar B., (2017) Nonlocal Vibration Analysis of Fluid Conveying Single-Walled Carbon Nanotube with Magnetic Effects, *Rasayan J. Chem.*, 10(2), 643-651  
<http://dx.doi.org/10.7324/RJC.2017.1021669>
- [13] Salvatore Brischetto, Francesco Tornabene, Nicholas Fantuzzi and Michele Baccocchi (2015) Refined 2D and Exact 3D Shell Models for the Free Vibration Analysis of Single- and Double-Walled Carbon Nanotubes, *Technologies*, 3, 259-284,  
<https://doi.org/10.3390/technologies304025>
- [14] Shaba A. I., Jiya M., Aiyesimi Y. M. and Mohammed A. A. (2021), Vibration of Single – Walled Carbon Nanotube on a Winkler Foundation with Magnetic Field Effect, *Science World Journal*, 16(4), 402-406.
- [15] Shota Kuwahara, Yuki Kuwahara and Hisanori Shinohara (2014) Quantitative Analysis of Isolated Single-Wall Carbon Nanotubes with Their Molar Absorbance Coefficients, *Journal of Nanomaterials* Vol. 2014, 7,  
<https://doi.org/10.1155/2014%2F262940>
- [16] Subrat Kumar Jena and Chakraverty S., (2018) Free Vibration Analysis of Single Walled Carbon Nanotube with Exponentially Varying Stiffness, Curved and Layer. *Struct.*, 5, 201–212,  
<http://dx.doi.org/10.1515/cls-2018-0015>
- [17] Subrat Kumar Jena, Chakraverty S., Mohammad Malikan, Francesco Tornabene (2019) Stability Analysis of Single-Walled Carbon Nanotubes Embedded in Winkler Foundation Placed in a Thermal Environment Considering the Surface Effect Using a New Refined Beam Theory, *Mechanics Based Design of Structures and Machines*, 1-27,  
<http://dx.doi.org/10.1080/15397734.2019.1698437>
- [18] Subrat Kumar Jena, Chakraverty S., Mohammad Malikan, Hamid Mohammad-Sedighi, (2020), Hygro-Magnetic Vibration of The Single-Walled Carbon Nanotube with Nonlinear Temperature Distribution Based on A Modified Beam Theory and Nonlocal Strain Gradient Model, *International Journal of Applied Mechanics*, 1-25,  
<http://dx.doi.org/10.1142/S1758825120500544>
- [19] Yinusa A. A., Sobamowo M. G., Adelaja A. O., Ojolo S. J., Waheed M. A., Usman M. A., Antonio Marcos de Oliveira Siqueira, Júlio César Costa Campos, Ridwan Ola-Gbadamosi (2024) Numerical investigation on the thermal-nanofluidic flow induced transverse and longitudinal vibrations of single and multi-walled branched nanotubes resting on nonlinear elastic foundations in a magnetic environment, *Partial Differential Equations in Applied Mathematics* 9, 100602,  
<https://doi.org/10.1016/j.padiiff.2023.100602>